Applied Energy 412 (2026) 127732

Contents lists available at ScienceDirect

Applied Energy

journal homepage: www.elsevier.com/locate/apenergy

Optimization of hydrogen supply operations for decarbonizing energy-intensive industries: A multi-timescale rolling horizon approach

Giulia Fede [a,*], Fabio Sgarbossa [a], Daniel F. Silva [b]

[a] Department of Mechanical and Industrial Engineering, Norwegian University of Science and Technology NTNU, Richard Birkelands vei 2B, 7034, Trondheim, Norway
[b] Department of Industrial and Systems Engineering, Auburn University, Auburn, AL 36849, USA

HIGHLIGHTS

- MINLP model of hydrogen production via electrolyzer and supply via truck delivery.
- Renewable availability and grid prices cause up to 60% variation in operating cost.
- Start-up transitions modeling helps reduce electrolyzer efficiency degradation.
- Rolling horizon limits cost rise to 2.47% under poor renewable energy forecasts.
- Grid-only backup is optimal in Italy when hydrogen delivery costs exceed 0.8 €/Nm^3.

GRAPHICAL ABSTRACT

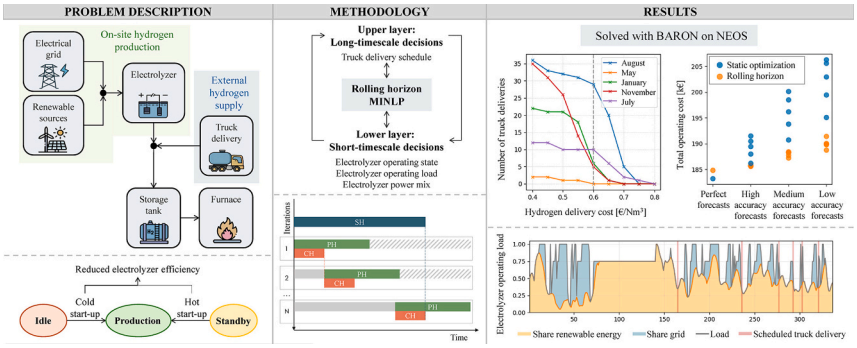

ARTICLE INFO

Keywords:
Power-to-hydrogen
Optimal hydrogen supply
Multi-state model
Rolling horizon
Renewable energy uncertainty
Energy-intensive industry
PEM electrolyzer

ABSTRACT

The adoption of green hydrogen, produced via water electrolysis using renewable energy sources, is a promising decarbonization strategy for energy-intensive industries. However, the feasibility of this transition depends on the economic viability of hydrogen supply and the ability to ensure a stable hydrogen supply under fluctuating and uncertain renewable energy availability. This study develops a Mixed-Integer Nonlinear Programming (MINLP) model to optimize hydrogen supply operations. On-site hydrogen production is supported by grid electricity purchases and complemented by external green hydrogen truck deliveries to ensure the continuous fulfillment of hydrogen demand in industrial furnaces. The model captures key electrolyzer operational dynamics, including variable loads, state transitions, and stack efficiency degradation. The formulation is embedded in a multi-timescale framework that accounts for different decision frequencies and implementation lead times of electrolyzer operations and external hydrogen delivery. The problem is solved using a rolling horizon approach to reduce reliance on long-term forecasts and enable reactive scheduling of hydrogen supply operations under renewable energy uncertainty. Results indicate that seasonal variations in renewable energy availability and grid electricity prices can cause operating cost differences of up to 60%. In contrast, renewable energy forecast inaccuracies result in cost variations limited to 2.47% under the rolling horizon approach, which achieves operating cost reductions of up to 4.15% compared to static optimization, demonstrating the robustness and relevance of the proposed framework. The use of real historical forecast datasets or the integration of forecasting algorithms represents an interesting direction for future research.

* Corresponding author.
E-mail address: giulia.fede@ntnu.no (G. Fede).

https://doi.org/10.1016/j.apenergy.2026.127732
Received 4 January 2026; Received in revised form 23 February 2026; Accepted 14 March 2026
Available online 20 March 2026

Nomenclature

Set

$t \in PH$	Time intervals included in the current prediction horizon

Parameters

D	Hydrogen demand from furnace (Nm^3/h)
η^n	Electrolyzer nominal efficiency
η^l	Electrolyzer minimum efficiency
LHV	Lower heating value hydrogen (kWh/Nm^3)
P	Power rated electrolyzer (kW)
L^u	Maximum operating load electrolyzer
L^l	Minimum operating load electrolyzer
P^s	Standby electricity consumption factor electrolyzer
c^r	Unitary renewable electricity consumption cost (€/kWh)
ε^g	Penalty cost electrical grid (€/kWh)
c^w	Unitary water consumption cost (€/Nm^3)
ρ	Voltage increase effect on electrolyzer efficiency
ΔV^h	Voltage increase from hot start-up (V)
ΔV^c	Voltage increase from cold start-up (V)
I^u	Maximum hydrogen level in storage tank (Nm^3)
I^l	Minimum hydrogen level in storage tank (Nm^3)
h	Hydrogen holding cost (€/Nm^3)
Δt	Time step (h)
c^s	Stack replacement cost (€)
C^T	Hydrogen capacity truck (Nm^3)
c^T	Unitary hydrogen delivery cost (€/Nm^3)
c^u	Labor cost for truck unloading (€)
p_0	Initial value of the production state variable at interval $t = 0$
s_0	Initial value of the standby state variable at interval $t = 0$
i_0	Initial value of the idle state variable at interval $t = 0$
I_0	Hydrogen inventory level at interval $t = 0$ (Nm^3)
η_0	Initial electrolyzer efficiency at interval $t = 0$

Continuous variables

L_t	Operating load electrolyzer at interval t
H_t^e	Hydrogen production rate from electrolyzer at interval t (Nm^3/h)
P_t^e	Hourly electricity consumption electrolyzer at interval t (kW)
η_t	Electrolyzer efficiency considering degradation at interval t
I_t	Hydrogen level in storage tank at the end of interval t (Nm^3)
I_t^i	Hydrogen input flow to the storage tank at interval t (Nm^3/h)
I_t^o	Hydrogen output flow from the storage tank at interval t (Nm^3/h)
$P_t^{r,u}$	Available hourly electricity from renewable sources at interval t (kW)
P_t^r	Consumed hourly electricity from renewable sources at interval t (kW)
P_t^g	Consumed hourly grid electricity at interval t (kW)
c_t^g	Unitary grid electricity consumption cost (€/kWh)

Binary variables

p_t	1 if electrolyzer is in production state at interval t; 0 otherwise
s_t	1 if electrolyzer is in standby state at interval t; 0 otherwise
i_t	1 if electrolyzer is in idle state at interval t; 0 otherwise
H_t	1 if a hot start-up transition occurs at interval t; 0 otherwise
C_t	1 if a cold start-up transition occurs at interval t; 0 otherwise
T_t	1 if truck arrival is scheduled at interval t; 0 otherwise

1. Introduction

1.1. Background and motivation

Energy-intensive industries, such as the glass, steel and aluminum sectors, are responsible for approximately 30% of global greenhouse gas emissions [1], therefore representing a significant target for global decarbonization efforts. High-temperature heating processes in industrial furnaces account for about half of these emissions, reflecting the current reliance on fossil fuel combustion, such as natural gas, to meet the process heat requirements [2]. Fuel switching to hydrogen constitutes a key decarbonization strategy, as hydrogen combustion enables high-temperature heat generation without direct emissions [3].

Among the primary technologies for hydrogen production, water electrolysis relies on electricity to split water into hydrogen and oxygen, therefore, its economic and environmental performance is highly dependent on the composition of the power mix adopted. When powered solely by grid electricity, the associated indirect emissions can exceed those of conventional natural gas-based operations [4], thereby offsetting the decarbonization benefits that the transition seeks to achieve. Conversely, the exclusive use of renewable energy sources represents the ideal scenario, yielding minimal indirect emissions.

However, the inherent intermittency of renewable energy sources poses a major challenge for hydrogen supply operations, defined in this study as the coordinated set of activities for supplying hydrogen to industrial furnaces, managed at the plant level by energy-intensive manufacturers undergoing the hydrogen transition. On one hand, fluctuations in power input conflict with the optimal operating conditions of electrolyzers, as frequent start-up transitions significantly accelerate stack degradation and consequently reduce overall hydrogen production efficiency [5]. On the other hand, they create a mismatch with the continuous fuel demand typical of energy-intensive industries [6]. When renewable energy availability is sufficiently high on a cumulative basis, this challenge can be mitigated through design choices, including the integration and appropriate sizing of buffer units such as batteries and hydrogen storage [7]. Even under these conditions, however, ensuring consistent alignment with process demand solely through buffers often requires oversizing these components, leading to high capital costs and substantial underutilization under average operating conditions [4]. A complementary approach to addressing fluctuations in renewable energy availability, which becomes essential in contexts with constrained renewable energy supply and limited opportunities for local infrastructure expansion, is the use of backup options, such as grid backup [6]. Previous studies have shown that, depending on the local context and electricity market conditions, partial reliance on grid electricity can effectively mitigate renewable energy variability and ensure a stable hydrogen supply [8]. At the same time, this approach can increase electrolyzer utilization and reduce start-up transitions [9], thus preventing accelerated degradation. This backup option is particularly beneficial in regions with high integration of renewable energy sources into the electrical grid (e.g., the Nordic countries), where reliance on grid electricity does not entail the high indirect emissions discussed above. Another option, supported by growing investments in green hydrogen production technologies, is to complement on-site production with external green hydrogen deliveries, for instance by means of truck transport [10]. This hydrogen supply backup option may become economically attractive under high electricity prices or in regions with high grid carbon intensity (e.g., many regions of the United States), particularly when coupled with rising carbon tax projections.

While the integration of buffer units and/or the use of backup options can help mitigate limited renewable energy availability and its inherent variability, another major challenge persists in the

management of hydrogen supply operations, namely the intrinsic uncertainty associated with renewable energy generation and electricity price volatility, which make future conditions difficult to forecast and can significantly affect hydrogen supply performance [11]. As a result, assuming perfect foresight of future renewable energy availability and electricity prices when scheduling hydrogen supply operations may produce infeasible or suboptimal plans, as actual conditions may deviate from forecasts. In this context, adopting reactive optimization approaches, such as rolling horizon methods, which support dynamic rescheduling as updated information becomes available, can help cope with the underlying uncertainty and improve the robustness and feasibility of the resulting hydrogen supply operation schedules [12].

1.2. Aim of the study and contributions

In line with the challenges and considerations outlined above, this study aims to develop a dynamic scheduling optimization framework for hydrogen supply operations that integrates on-site hydrogen production with external deliveries, incorporates grid electricity purchasing, explicitly models electrolyzer degradation, and maintains robustness to uncertainty in renewable energy availability and grid electricity prices.

The main contributions of this study are as follows:

- The development of a comprehensive MINLP formulation that captures detailed Proton Exchange Membrane (PEM) electrolyzer behavior, including multiple operational states, variable operating loads, hot and cold start-up transitions with associated efficiency degradation, while also modeling hydrogen storage dynamics, grid electricity purchases, and external green hydrogen supply via truck deliveries to ensure continuous fulfillment of hydrogen demand and sustained electrolyzer operations.
- The use of a multi-timescale rolling horizon solution approach, in which the same MINLP formulation is solved through rolling horizon optimization at two distinct layers, allowing long-timescale decisions (e.g., truck deliveries) and short-timescale decisions (e.g., electrolyzer operations) to be optimized at different frequencies in accordance with their differing implementation lead times, while reducing the reliance on long-term forecasts and enabling dynamic and reactive scheduling of hydrogen supply operations under uncertainty in renewable energy availability.
- The development of a novel trade-off analysis between grid electricity purchases and external green hydrogen deliveries via truck transport as backup options for ensuring continuous hydrogen demand fulfillment, evaluated through sensitivity analyses of grid penalty costs and hydrogen delivery costs.
- The evaluation of the robustness of the proposed optimization framework to forecast inaccuracies in renewable energy availability, supported by a comparative analysis against a static optimization approach under both perfect and imperfect forecast scenarios.

To achieve the research aims, the remainder of the paper is structured as follows. Section 2 presents the relevant literature, positions this study within the existing work, and highlights its novelty. The problem formulation is detailed in Section 3 and includes a description of the system under investigation, the decision variables, and the developed MINLP formulation with its objective function and constraints representing system behavior. This section also introduces the overall multi-timescale rolling horizon optimization framework into which the proposed mathematical formulation is integrated. The case study is presented in Section 4, which outlines the main assumptions, parameters, and input data. Section 5 presents and discusses the results obtained for the reference scheduling period, complemented by sensitivity analyses across different periods and input parameters to examine the trade-offs among backup options. The impact of forecast accuracy on the optimal results is also examined, and the benefits of adopting a rolling horizon approach under imperfect knowledge are quantified. Lastly, Section 6 concludes the paper by summarizing the main findings and outlining the main limitations and future research directions.

2. Relevant literature

A considerable body of research has focused on the optimization of hydrogen supply operations, especially in the context of electrolyzer-based hydrogen production, with the most relevant works summarized below.

Liao et al. [13] investigate the optimal operation of a wind-powered electrolyzer with the objective of maximizing revenues from electricity and hydrogen sales, without imposing any hydrogen demand constraint. As a result, neither buffer units nor backup strategies are required. The same objective function is considered by Matute et al. [14], who explore a photovoltaic-powered electrolyzer supported by grid electricity to meet a specific hydrogen demand. Zheng et al. [15] adopt the same objective function for a wind-powered electrolyzer and examine both fixed and flexible hydrogen production cases, showing that the latter enables reduced operating costs. In this case, grid electricity is allowed, and a hydrogen storage tank is integrated into the system. All three studies adopt a three-state operational model for the electrolyzer, including the associated state transitions. Stack degradation is explicitly accounted for in Zheng et al. [15] by assigning cost terms to hot and cold start-up transitions, while Matute et al. [14] model stack degradation using a linear cost based on cumulative operating hours. However, none of these studies investigates the stack degradation effect in terms of electrolyzer efficiency losses. The optimization problem in all cases is formulated as a static optimization model and solved with a 15-min or a one-hour time resolution.

Zheng et al. [16] investigate operational strategies for an off-grid multi-electrolyzer system powered by wind, aiming to minimize hydrogen production costs without imposing a hydrogen demand constraint. Similarly, Ibáñez-Rioja et al. [17] also neglect hydrogen demand requirements while minimizing total costs for an off-grid electrolyzer system powered by wind and solar energy, including capital expenditures. In this case, the inclusion of a battery as a buffer unit enables higher electrolyzer utilization. Zheng et al. [16] adopt a three-state operational model and account for electrolyzer efficiency losses due to frequent start-up transitions, whereas Ibáñez-Rioja et al. [17] employ a simplified on-off electrolyzer model, in which efficiency degradation is linked solely to cumulative operating hours. Given the long-term perspective of their analysis, stack replacements and the associated capital costs are also considered. Guo et al. [9] also investigate an off-grid electrolyzer system powered by wind and solar energy, with the objective of minimizing total investment and production costs. Unlike Ibáñez-Rioja et al. [17], a hydrogen demand constraint is imposed, which necessitates the integration of a hydrogen storage tank as an additional buffer unit. A three-state operational model is adopted; however, only cold start-up transitions are considered, and stack degradation effects are neglected. In all cases, the optimization problem is again formulated as a static optimization model and solved using a five-minute or a one-hour time resolution. The potential benefits of adopting backup options are neglected in these studies.

Bukar et al. [18] jointly investigate the design and operation of a photovoltaic-powered electrolyzer system using an on-off electrolyzer model, while including a cost term to account for stack degradation. Trapani et al. [10] address the same objective, but simulate system operation through a predefined control strategy rather than explicitly optimizing operational decisions. These studies rely on a more comprehensive set of buffer units and backup options to ensure demand fulfillment. In particular, Bukar et al. [18] allow grid-supported operation and integrate both a battery and a hydrogen storage tank into the system, whereas Trapani et al. [10] consider only a hydrogen storage tank as a buffer unit, but complement on-site production supported by grid electricity with external deliveries of grey hydrogen. Although both studies adopt a common time resolution of one hour, their optimization

Table 1
Relevant literature on optimization of hydrogen supply operations.

Author	Aim	Hydrogen demand constraint	Optimization approach	EL operational states	Backup option(s)	Buffer unit(s)	Stack degradation
Liao et al. [13]	Operations optimization	No	Static optimization	Production, Standby, Idle	No	No	No
Matute at [14]	Operations optimization	Yes	Static optimization	Production, Standby, Idle	Grid	No	Cost
Zheng et al. [15]	Operations optimization	Yes/No	Static optimization	Production, Standby, Idle	Grid	Tank	Cost
Zheng et al. [16]	Operational strategies optimization	No	Static optimization	Production, Standby, Idle	No	No	Efficiency
Ibáñez-Rioja et al. [17]	Operations and design optimization	No	Static optimization	On, Off	No	Battery	Efficiency
Guo et al. [9]	Operations and design optimization	Yes	Static optimization	Production, Standby, Idle	No/Grid	Battery and tank	No
Bukar et al. [18]	Operations and design optimization	Yes	Rolling horizon	On, Off	Grid	Battery and tank	Cost
Trapani et al. [10]	Operations and design optimization	Yes	Static optimization	On, Off	Grid and truck deliveries	Tank	No
Mößle et al. [19]	Operations optimization	Yes	Dynamic programming	On, Off	Grid	Battery	Cost
Peng et al. [20]	Operations optimization	No	Stochastic optimization	On, Off	Grid	Battery	No
This study	Operations optimization	Yes	Rolling horizon	Production, Standby, Idle	Grid and truck deliveries	Tank	Cost and efficiency

approaches differ. Trapani et al. [10] formulate a static optimization problem, complemented by a metaheuristic approach to identify optimal system designs under different carbon reduction targets. In contrast, Bukar et al. [18] employ a rolling horizon approach to address uncertainties in key input parameters, including hydrogen demand, electricity demand, solar irradiance, and electricity prices, whose updated values are assumed to be obtained through forecasting algorithms. The use of a simplified on-off model in these studies does not enable the assessment of the effect of state transitions on stack degradation; losses in electrolyzer efficiency based on electrolyzer operations are not investigated either.

Non-static optimization approaches are employed by Mößle et al. [19] and Peng et al. [20], both of whom aim to optimize electrolyzer operations to minimize total operating costs. Mößle et al. [19] employ a dynamic programming approach, sequentially solving the optimization problem to reflect day-ahead electricity market conditions, as the electrolyzer is powered exclusively by grid electricity. In contrast, Peng et al. [20] adopt a stochastic optimization framework to address uncertainty in renewable energy availability, as they consider an electrolyzer supplied by wind and solar energy sources with limited grid electricity support. Both studies adopt a simplified on-off electrolyzer model with a one-hour time resolution and integrate battery energy storage as a buffer unit. However, only Mößle et al. [19] impose a hydrogen production requirement. Regarding degradation modeling, Mößle et al. [19] integrate the different stack degradation effects associated with different operating conditions through cost terms, whereas Peng et al. [20] do not explicitly model stack degradation, but they impose a limit on the number of start-up transitions to prevent accelerated degradation. However, the effect of state transitions on electrolyzer degradation is not considered in these studies.

Table 1 summarizes the relevant literature discussed above.

No dominant approach emerges with respect to electrolyzer operation modeling. While several studies adopt a three-state representation, an equal number of papers rely on a simpler on-off formulation. Similarly, approaches to stack degradation modeling vary considerably. Some authors incorporate degradation through a cost term, others represent it as an efficiency reduction, while some omit it entirely. As for buffer units and backup options, these are entirely excluded in some cases where no hydrogen demand constraint is imposed. When the problem includes meeting a specified hydrogen demand, grid support is always incorporated, underscoring the challenges of operating such systems solely on renewable energy. In most cases, this is complemented by the inclusion of buffer units, typically a battery and/or a hydrogen storage tank. Finally, the use of an hourly time resolution is the most common choice in the literature, although the problem horizon varies considerably across studies.

Regarding methodological approaches, most studies employ static optimization, in which the entire scheduling horizon is solved simultaneously under the assumption of full foresight. Mößle et al. [19] represent an exception by adopting dynamic programming. Their formulation decomposes the weekly optimization problem into sequential daily subproblems, consistent with the day-ahead structure of electricity markets. Nevertheless, each day's schedule is solved only once and remains unchanged during the day. In contrast, Bukar et al. [18] adopt a rolling horizon approach, thereby enabling dynamic re-optimization of the schedule on an hourly basis as updated information becomes available. This allows the model to address additional sources of intraday uncertainty, including renewable energy availability. With the same objective, Peng et al. [20] employ a stochastic optimization approach, generating multiple scenarios of renewable energy availability to explicitly account for its uncertainty. While stochastic optimization provides a rigorous framework for decision-making under uncertainty and ensures feasibility across the considered scenarios, the construction of realistic and representative scenarios of renewable energy availability is challenging. Moreover, this methodology can lead to conservative solutions, as the model must also accommodate rare or

extreme realizations of renewable energy availability. For this reason, the present study adopts a rolling horizon approach to address uncertainty in renewable energy availability.

Unlike Bukar et al. [18], the present study adopts a three-state electrolyzer model that explicitly captures the impact of start-up transitions on hydrogen production efficiency. Furthermore, an additional backup option beyond grid support is incorporated, namely the external delivery of hydrogen via truck transport, as also considered in Trapani et al. [10]. However, instead of modeling external hydrogen supply as continuously available, the present study considers external green hydrogen delivery through truck deliveries with fixed capacity that require advance scheduling. This modeling approach is more consistent with studies from the external hydrogen supplier perspective [21]. More specifically, to account for the longer implementation lead times associated with truck deliveries relative to electrolyzer operational decisions, the present study integrates the rolling horizon optimization approach within a multi-timescale framework. A similar solution methodology has been adopted in broader energy system scheduling problems. For example, [22] proposes a multi-timescale rolling horizon framework integrated with distributionally robust optimization for the optimal scheduling of a hybrid energy storage system under renewable energy uncertainty. However, the sensitivity of the scheduling results to different levels of forecast accuracy is not explicitly analyzed. To address uncertainty in renewable energy, [23,24] introduce multi-timescale frameworks for scheduling integrated energy systems, incorporating hydrogen as an energy carrier. While [23] adopts a multi-timescale approach integrated with stochastic optimization to refine scheduling decisions in the lower layers by shortening forecast horizons, [24] combines a multi-timescale framework with deep reinforcement learning to monitor and locally adjust intra-day scheduling decisions only when significant forecast deviations are detected, rather than fully re-optimizing scheduling decisions based on observed realizations. While these studies make important methodological contributions to multi-timescale scheduling of integrated energy systems, their multi-timescale structures are primarily motivated by renewable energy uncertainty, rather than by the need to coordinate operational decisions with different implementation lead times. Furthermore, to the best of our knowledge, a similar multi-timescale optimization framework has not yet been specifically applied to the scheduling of hydrogen supply industrial operations.

3. Problem formulation

This section presents the overall problem formulation. Section 3.1 describes the system under investigation, while Section 3.2 introduces the key operational decisions. Section 3.3 details the mathematical formulation developed to represent the system's behavior, and Section 0 explains the multi-timescale rolling horizon framework within which the formulation is integrated.

3.1. System description

Fig. 1 presents a schematic representation of the system under investigation. On-site hydrogen production is achieved through water electrolysis using a PEM electrolyzer, with water and electricity serving as the main input resources. Electricity can be supplied to the electrolyzer from renewable energy sources and, when necessary, from the electrical grid. The electrolyzer operates in three distinct states: production, standby, and idle. In the production state, the electrolyzer generates hydrogen and consumes electricity according to its operating load. In standby state, minimal electricity consumption persists without hydrogen production, whereas in the idle state, neither electricity consumption nor hydrogen generation occurs. Transitions from idle or standby to production are referred to as cold and hot start-up transitions, respectively. Each start-up will negatively affect the electrolyzer lifetime, as start-up transitions significantly accelerate stack degradation [6,15]. A more detailed description of PEM electrolyzer operational characteristics can be found in Wang et al. [25]. To ensure a stable hydrogen supply under variable operating conditions, on-site hydrogen production can be complemented by an external hydrogen supply. In this study, compressed green hydrogen delivered by truck is considered as an additional supply source. A storage tank is installed on-site to accommodate both hydrogen supply flows, serving as a buffer to further ensure a continuous hydrogen supply to the industrial furnace. The stored hydrogen is ultimately used to meet the furnace's fuel demand for the combustion process.

3.2. Decision variables

Considering the system under investigation, the main decisions to be optimized for the management of hydrogen supply operations concern when to schedule truck deliveries and how to operate the electrolyzer, specifically when to switch between operational states (idle, standby, and production), at which load to run the electrolyzer during production, and which mix of renewable energy and grid electricity to adopt. These decisions are characterized by different implementation lead times, i.e., the time required between decision-making and actual execution. Truck deliveries are managed externally and involve hydrogen production and distribution planning by the supplier, with lead times that vary depending on the producer's characteristics and location, but are generally longer than those associated with electrolyzer operations. The latter are carried out on-site and are directly controlled by the energy-intensive manufacturer, allowing frequent adjustments to operating parameters in response to changing external conditions. To account for these differences in implementation lead time, the decisions are categorized as follows:

- Long-timescale decisions deal with the optimal truck delivery schedule on a daily to multi-day basis.

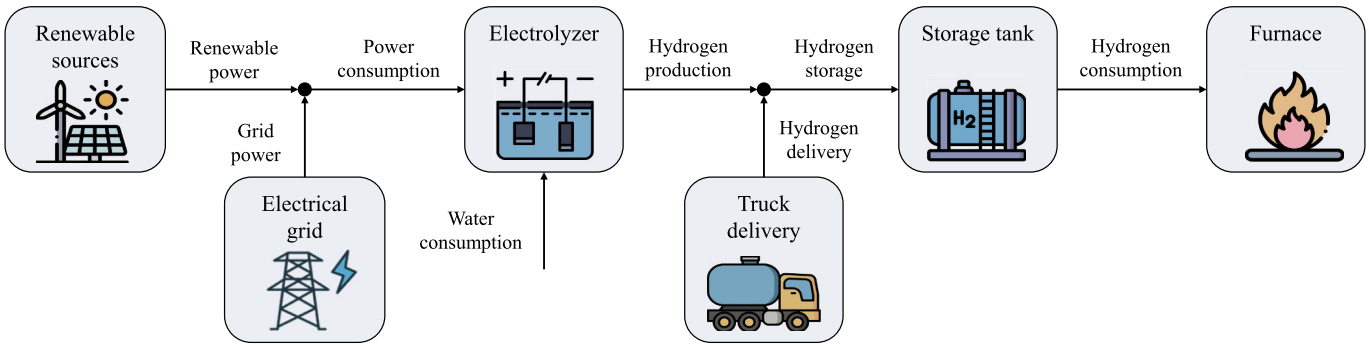

Fig. 1. Schematic representation of the system under investigation.

Table 2
Model decision variables.

Notation	Description	Unit of measure	Timescale
T_t	Binary variable taking value 1 if a truck arrival is scheduled at interval t; 0 otherwise	–	Long-timescale
p_t	Binary variable taking value 1 if the electrolyzer is in the production state at interval t; 0 otherwise	–	Short-timescale
s_t	Binary variable taking value 1 if the electrolyzer is in the standby state at interval t; 0 otherwise	–	Short-timescale
i_t	Binary variable taking value 1 if the electrolyzer is in the idle state at interval t; 0 otherwise	–	Short-timescale
L_t	Operating load of the electrolyzer at internal t	–	Short-timescale
P_t^r	Hourly renewable power consumption of the electrolyzer at interval t	kW	Short-timescale
P_t^g	Hourly grid power consumption of the electrolyzer at interval t	kW	Short-timescale

- Short-timescale decisions involve determining the optimal electrolyzer operation on an hourly basis.

These decisions are formulated as decision variables. Table 2 systematically presents them, including their notation, description, and unit of measure where applicable. Note that, at this stage, the index t represents a generic time interval, with additional details on its length provided later.

3.3. MINLP formulation

A MINLP problem is formulated to represent the behavior of the system, as it includes both continuous and integer variables and comprises linear as well as nonlinear constraints. This section details the MINLP formulation, beginning with the objective function and associated cost components in Section 3.3.1, followed by the constraints, grouped by their role in the model in Sections 3.3.2 through 3.3.7.

3.3.1. Objective function

The objective function aims to minimize the overall operating cost (OC) of the system, as defined in (1), which accounts for the costs related to electricity consumption (EC), water consumption (WC), hydrogen inventory (IC), electrolyzer degradation (DC), and truck deliveries (TC).

$$\min OC = EC + WC + IC + DC + TC \tag{1}$$

EC is estimated as in (2), based on the hourly electricity consumption of the electrolyzer. The cost function distinguishes between the power supplied by renewables P_t^r, whose hourly consumption cost is c^r, and the power drawn from the electrical grid P_t^g, whose hourly consumption cost corresponds to the market price c_t^g, plus a time-constant penalty per kWh ε^g, which can represent carbon taxes or other costs associated with the use of fossil fuels. Note that Δt represents the length of the time interval t in hours.

$$EC = \sum_{t\in PH} P_t^r \bullet \Delta t \bullet c^r + P_t^g \bullet \Delta t \bullet \left(c_t^g + \varepsilon^g\right) \tag{2}$$

WC is calculated as in (3), considering the hourly hydrogen production of the electrolyzer H_t^e, and the unit water consumption c^w.

$$WC = \sum_{t\in PH} H_t^e \bullet \Delta t \bullet c^w \tag{3}$$

IC is estimated starting from the hydrogen level in the storage tank I_t, and considering an inventory holding cost h, as follows:

$$IC = \sum_{t\in PH} I_t \bullet h \tag{4}$$

Regarding DC estimation, the cost function accounts for the reduction in electrolyzer efficiency resulting from start-up transitions. Each hot start-up ($H_t = 1$) and cold start-up ($C_t = 1$) causes an increase in the operating voltage of the electrolyzer stack equal to ΔV^H and ΔV^C, respectively. The effect of this operating voltage increase on the electrolyzer efficiency reduction is represented by the parameter ρ. Therefore, (5) quantifies the partial contribution of each start-up transition to the overall efficiency degradation of the electrolyzer (i.e., $\eta^n - \eta^l$), which is then converted into a cost by including the stack replacement expense c^s.

$$DC = \sum_{t\in PH} \left(H_t \bullet \Delta V^H + C_t \bullet \Delta V^C\right) \bullet \frac{\rho}{\eta^n - \eta^l} \bullet c^s \tag{5}$$

Lastly, TC includes, for each delivery, the cost of the hydrogen delivered, whose total quantity is equal to the truck capacity C^T and whose unit price is c^T, as well as the additional labor expense c^u associated with qualified operators required to perform the truck unloading, as follows:

$$TC = \sum_{t\in PH} T_t \bullet \left(C^T \bullet c^T + c^u\right) \tag{6}$$

3.3.2. Electrolyzer production constraints

The hydrogen production flow from the PEM electrolyzer is computed using the nonlinear constraint (7). Hydrogen is produced only when the electrolyzer is in the production state, and the resulting production flow depends on the rated power P, the operating load L_t, and the current efficiency η_t. The lower heating value LHV is used to convert the energy term into a hydrogen flow rate.

$$H_t^e = \frac{P \bullet L_t \bullet \eta_t}{LHV} \qquad \forall t \in PH \tag{7}$$

The electrolyzer can operate only within a specific load range, delimited by the lower bound L^l and the upper bound L^u. These limits are imposed through constraints (8) and (9), which also impose that L_t is zero when the electrolyzer is not in the production state (i.e., $p_t = 0$)

$$L_t \geq L^l \bullet p_t \qquad \forall t \in PH \tag{8}$$

$$L_t \leq L^u \bullet p_t \qquad \forall t \in PH \tag{9}$$

3.3.3. Electrolyzer power consumption constraints

The electricity consumption of the electrolyzer is determined using (10). A different fraction of the rated power P is applied depending on the operational state: the operating load L_t when the electrolyzer is in production, and the standby power consumption factor P^s when it is on standby ($s_t = 1$).

$$P_t^e = P \bullet (L_t + P^s \bullet s_t) \qquad \forall t \in PH \tag{10}$$

The following balance equation guarantees that the power consumed by the electrolyzer is supplied from renewable energy P_t^r and/or grid P_t^g:

$$P_t^e = P_t^r + P_t^g \qquad \forall t \in PH \tag{11}$$

Lastly, renewable power consumption P_t^r cannot exceed the maximum renewable energy available $P_t^{r,u}$:

$$P_t^r \leq P_t^{r,u} \qquad \forall t \in PH \tag{12}$$

3.3.4. Electrolyzer operational state constraints

The operational state of the electrolyzer is restricted to only one state between production ($p_t = 1$), standby ($s_t = 1$), and idle ($i_t = 1$) with the following constraint:

$$p_t + s_t + i_t = 1 \qquad \forall t \in PH \tag{13}$$

Additionally, the transition from the idle state to the standby state is constrained by (14) and (15), as this transition is considered unfavorable.

$$i_0 + s_t \leq 1 \qquad t = 1 \tag{14}$$

$$i_{t-1} + s_t \leq 1 \qquad \forall t \in PH : t > 1 \tag{15}$$

The transition from standby to production, referred to as a hot start-up H_t, is modeled as follows:

$$H_t = p_t \bullet s_0 \qquad t = 1 \tag{16}$$

$$H_t = p_t \bullet s_{t-1} \qquad \forall t \in PH : t > 1 \tag{17}$$

Similarly, the transition from idle to production, denoted as a cold start-up C_t, is accounted for as follows:

$$C_t = p_t \bullet i_0 \qquad t = 1 \tag{18}$$

$$C_t = p_t \bullet i_{t-1} \qquad \forall t \in PH : t > 1 \tag{19}$$

Constraints (16)–(19) associated with the hot and cold start-up transitions are also nonlinear.

3.3.5. Electrolyzer degradation constraints

The current electrolyzer efficiency is estimated as in (20) and (21). As discussed in Section 3.3.1 in the context of electrolyzer degradation cost estimation, efficiency decreases following start-up transitions, and the relationship between the associated increase in operating voltage and the resulting efficiency loss is captured by the parameter ρ. As stack replacement is out of scope in this study, the electrolyzer efficiency only decreases over time.

$$\eta_t = \eta_0 - \rho \bullet \left(H_t \bullet \Delta V^H + C_t \bullet \Delta V^C\right) \qquad t = 1 \tag{20}$$

$$\eta_t = \eta_{t-1} - \rho \bullet \left(H_t \bullet \Delta V^H + C_t \bullet \Delta V^C\right) \qquad \forall t \in PH : t > 1 \tag{21}$$

3.3.6. Hydrogen supply and demand constraints

The hydrogen inflow to the storage tank is computed as in (22) and corresponds to the total hydrogen supplied, which includes the hydrogen produced by the electrolyzer H_t^e and, when a delivery occurs ($T_t = 1$), the hydrogen delivered by the truck C^T.

$$I_t^i = H_t^e + T_t \bullet C^T \qquad \forall t \in PH \tag{22}$$

Additionally, the hydrogen outflow from the storage tank must satisfy the furnace's hydrogen consumption demand D, as follows:

$$I_t^o \geq D \qquad \forall t \in PH \tag{23}$$

3.3.7. Hydrogen storage constraints

The hydrogen inventory level in the storage tank I_t is estimated by using traditional inventory balance equations:

$$I_t = I_0 + I_t^i \bullet \Delta t - I_t^o \bullet \Delta t \qquad t = 1 \tag{24}$$

$$I_t = I_{t-1} + I_t^i \bullet \Delta t - I_t^o \bullet \Delta t \qquad \forall t \in PH : t > 1 \tag{25}$$

Additionally, the amount of hydrogen stored must remain between the maximum allowable level I^u, which depends on the storage capacity of the tank, and a minimum level I^l. These limits are imposed through the following constraints:

$$I_t \leq I^u \qquad \forall t \in PH \tag{26}$$

$$I_t \geq I^l \qquad \forall t \in PH \tag{27}$$

Lastly, all continuous variables included in the formulation are defined as non-negative.

3.4. Multi-timescale rolling horizon approach

The proposed MINLP formulation is embedded in a multi-timescale rolling horizon framework. The multi-timescale structure, consisting of an upper and a lower layer, accounts for different decision frequencies and implementation lead times across decision variables, while the rolling horizon approach reduces reliance on long-term forecasts and addresses operational variability and uncertainty. Specifically, the rolling horizon approach consists of iteratively solving an optimization problem while advancing the optimization window at each iteration. It typically requires the definition of three time horizons: a scheduling horizon (*SH*), which defines the overall period over which decisions are optimized; a prediction horizon (*PH*), over which future conditions are anticipated and incorporated into the optimization; and a control horizon (*CH*), corresponding to the time interval during which decisions are implemented before the optimization problem is re-solved. In this study, the rolling horizon framework is applied to both the upper and lower layers. Accordingly, the notation SH^{UL}, PH^{UL}, and CH^{UL}, as well as SH^{LL}, PH^{LL}, and CH^{LL} is introduced to denote the scheduling, prediction, and control horizons associated with the upper and lower layers, respectively. In both layers, the same MINLP formulation presented in Section 3.3 is solved using a common temporal resolution (e.g., one hour), while different horizon lengths and sets of decision variables are defined for each layer. These differences are explained in detail in the remainder of this section, which first describes the role of the upper layer and then that of the lower layer, highlighting the link between them.

Fig. 2 provides a schematic representation of the overall structure of the multi-timescale rolling horizon approach and includes specific assumptions regarding the time horizons used in the case study, which are used for illustrative purposes and to facilitate interpretation of the results. Some of these assumptions may vary depending on the application and the case investigated, as discussed below.

The upper layer is defined over a scheduling horizon SH^{UL} that coincides with the overall problem horizon, i.e., the period over which hydrogen supply operations are optimized, which may span several weeks or months depending on the application. At this level, the MINLP formulation optimizes long-timescale decisions, specifically determining whether a hydrogen truck delivery is scheduled at each time interval t ($T_t = 1$). Forecasts of uncertain inputs, such as renewable energy availability, are considered over the prediction horizon PH^{UL}, which may span several days depending on forecasting capabilities and the desired level of forecast accuracy, and are used to inform the optimization over the current control horizon CH^{UL}, set to one day.

Truck delivery decisions corresponding to the current control horizon CH^{UL} are implemented and not subject to re-optimization in subsequent upper layer iterations; these decisions are passed as fixed inputs to the lower layer optimization. Unlike a standard rolling horizon implementation, truck deliveries scheduled beyond CH^{UL} are also treated as committed and cannot be cancelled, reflecting the longer lead times associated with logistics operations and ensuring that planned deliveries are respected. Over the remaining portion of the prediction horizon PH^{UL} beyond CH^{UL}, these committed deliveries remain fixed, while additional truck deliveries may be scheduled in subsequent upper layer iterations as the optimization window advances.

The lower layer is defined over a scheduling horizon SH^{LL} equal to the upper layer control horizon CH^{UL}, and therefore covers one day. At this level, the MINLP formulation optimizes short-timescale decisions, including the operational state of the electrolyzer at each time interval t (p_t, s_t, and i_t), the electrolyzer operating load at interval t (L_t), and the energy mix used to power the electrolyzer at interval t (P_t^r and P_t^g) when the electrolyzer is in the production state ($p_t = 1$). Truck delivery decisions passed from the upper layer for the current CH^{UL} are treated as fixed inputs in the lower layer optimization over the scheduling horizon SH^{LL}. The length of the prediction horizon PH^{LL} coincides with that of the scheduling horizon SH^{LL}, whereas the control horizon CH^{LL} is

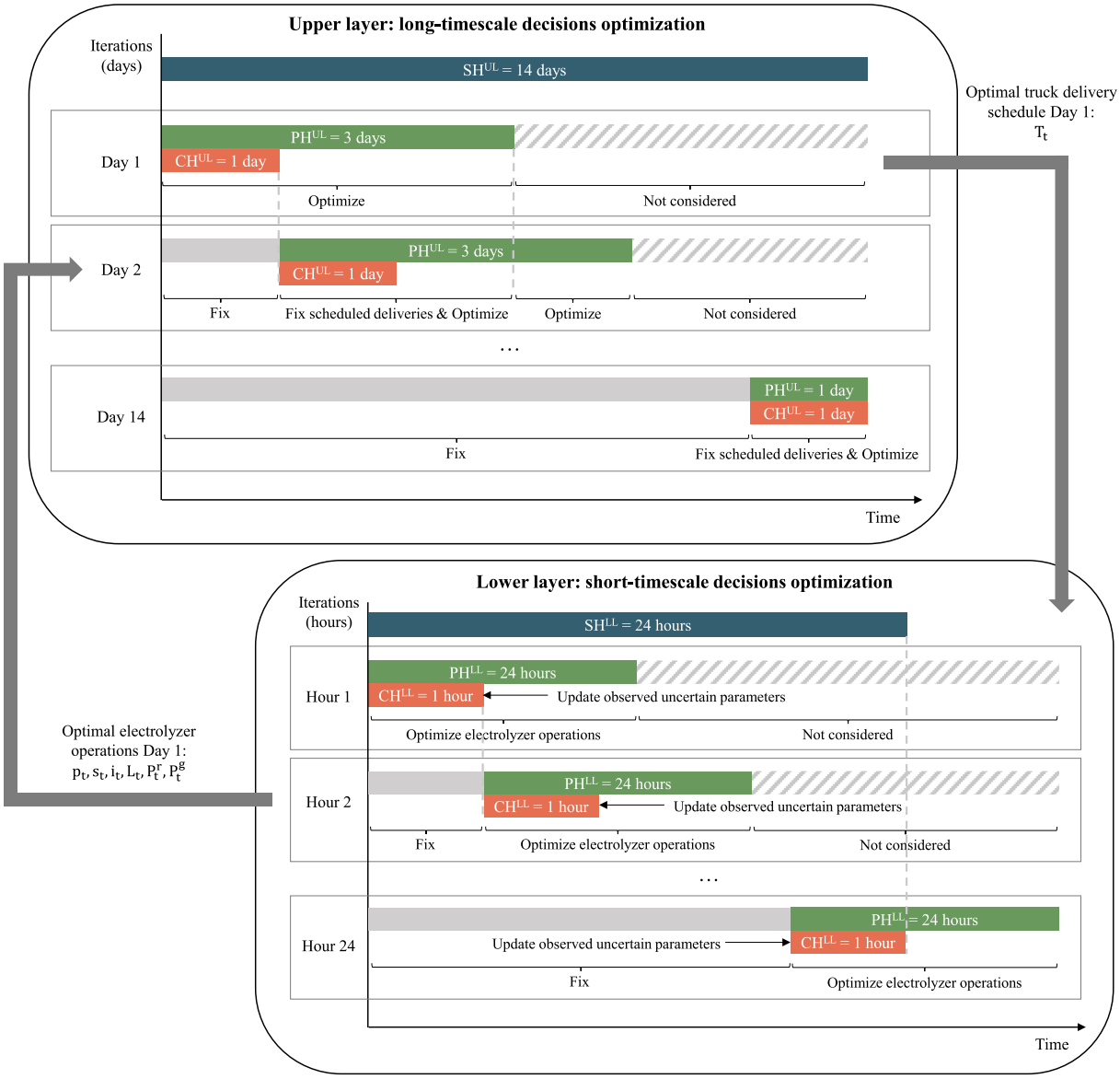

Fig. 2. Schematic representation of the multi-timescale rolling horizon approach.

significantly shorter than that considered in the upper layer, reflecting the higher decision frequency and greater flexibility in adjusting electrolyzer operations compared to external truck deliveries. The control horizon CH^{LL} may range from sub-hourly to multi-hour intervals, depending on the level of control that the energy-intensive manufacturer has over electrolyzer operating conditions. Additionally, observed values of uncertain parameters, such as renewable energy availability, are used over CH^{LL}, while forecasted values are retained over the remaining portion of PH^{LL}.

The optimization problem is solved iteratively until optimal electrolyzer operations are determined and implemented over the entire lower layer scheduling horizon SH^{LL}, corresponding to the current day. The resulting electrolyzer operating schedule is subsequently passed to the upper layer to define the initial conditions for the next iteration at that level and to either extend or re-optimize truck delivery decisions over the subsequent days within the new prediction horizon PH^{UL}.

Note that, due to the different lengths of the prediction horizons in the upper and lower layers, the set of time intervals $t \in PH$ included in the MINLP formulation refers to either PH^{UL} or PH^{LL}, depending on the layer in which the optimization problem is solved.

4. Case study

Among energy-intensive industries, the glass manufacturing sector has been selected as the focus of this study, as hydrogen combustion is considered one of the most promising decarbonization strategies for glass production [26], and initial testing has shown encouraging results in terms of combustion performance and final product quality [27]. However, ensuring a continuous and stable hydrogen supply remains one of the main challenges for its integration in glass manufacturing [28].

The overall scheduling horizon SH^{UL} is set to 14 days (i.e., 336 h), consistent with the typical planning period used in glass manufacturing for final product scheduling. As different glass products may have varying batch compositions, and thus different energy requirements for melting, this production schedule provides the basis for estimating the corresponding furnace energy demand and, consequently, the required hydrogen flow. In the upper layer, a three-day (i.e., 72 h) prediction horizon PH^{UL} is adopted, as it reflects the typical timeframe over which forecasts of renewable energy availability are available with acceptable accuracy, despite the inherent uncertainty. As discussed in the previous section, the upper layer control horizon CH^{UL} is set to one day (i.e., 24

h), reflecting the longer lead times for truck deliveries, and coincides with the lower layer scheduling horizon SH^{LL}. The lower layer prediction horizon PH^{LL} is set to and kept fixed at 24 h to prevent opportunistic model behavior (i.e., end-of-horizon effects) that could arise in the absence of visibility over future operational requirements. For instance, the model might otherwise determine that keeping the electrolyzer on standby is optimal, ignoring that a start-up will be needed in the following hours. Finally, the lower layer control horizon CH^{LL} is set to one hour, matching the temporal resolution of the MINLP formulation and aligning with common practice in the literature, while still enabling frequent updates of electrolyzer operating decisions based on newly observed external conditions.

A 10 MW PEM electrolyzer is chosen to ensure coverage of the average hydrogen demand, assumed equal to 1500 Nm^3/h, which has been estimated from the typical natural gas consumption in glass container manufacturing, taking into account the different lower heating values of the two fuels. PEM electrolyzers are characterized by a flexible operating load range, typically between 10% and 100% of their rated capacity, and a nominal efficiency of approximately 60%. A standby power consumption equal to 2% of the rated capacity is assumed [14]. A storage tank with a maximum capacity of 10,000 Nm^3 is included in the system to accommodate both on-site hydrogen production and external supply via truck delivery. Each truck delivery provides 7000 Nm^3 of hydrogen, with an unloading time of 1 h [29]. A minimum filling percentage is imposed for the storage tank, set at 10% of its maximum storage capacity, and is used to define the minimum allowable hydrogen inventory level. With regard to electrolyzer stack degradation dynamics, each hot and cold start-up transition is assumed to contribute to an increase in operating voltage of 1×10^{-5} V and 1×10^{-6} V, respectively [16]. The resulting impact of increased operating voltage on stack efficiency loss is quantified using an estimated degradation factor of 31.5 [5].

The analysis considers that the glass container facility is located in Italy; therefore, the input parameters for external conditions are defined based on this local context. Renewable energy availability is estimated using the wind energy model and input data from [30]. A value of 2.8 is selected for the ratio between installed wind power and electrolyzer capacity [30], while aggregated wind capacity factor data referring to 2014 are used. Grid electricity price data referring to 2024 are also incorporated into the model [31]. The selected years are considered reference periods for the respective input parameters, as their monthly mean values show minimal variation when compared with the corresponding monthly averages computed across several years.

Lastly, Table 3 shows the selected values for the economic parameters. To disincentivize the use of grid electricity, a penalty cost for the associated emissions is incorporated, reflecting both the economic and environmental impact of grid-based electrolysis. This cost parameter is estimated using the average carbon intensity of the electrical grid and the average carbon allowance price for 2024, equal to 0.274 $kgCO_2e$/kWh and 0.067 €/$kgCO_2$, respectively. Additionally, the cost associated with stack replacement is estimated assuming a value equal to 26.7% of the electrolyzer investment cost.

5. Results and discussion

The proposed MINLP formulation, integrated into the multi-timescale rolling horizon framework, has been implemented in GAMS 49.6.1 and solved using BARON 25.2.1 [40] through the NEOS server 6.0. All instances were solved to zero optimality gap. The average computational time per rolling horizon iteration is 1.43 s for the upper layer and 0.30 s for the lower layer, with corresponding maximum computational times of 3.61 s and 1.55 s, respectively (see Table 8 for detailed computational performance results).

5.1. Optimal results for the reference scheduling period under perfect knowledge

A first analysis is conducted under the assumption of perfect knowledge of renewable energy availability, so that the impact of operational decisions on process performance can be evaluated independently of forecasting accuracy. The model is applied to input data covering two consecutive weeks in July (5–18 July), which are used as the reference scheduling period. Fig. 3 illustrates the corresponding optimal hydrogen supply operations schedule.

Fig. 3.a presents the optimal electrolyzer operating schedule, showing both the hourly operating load and the respective contributions of renewable and grid to the overall power mix. Renewable power clearly dominates, accounting for 75% of total power consumption. The electrolyzer remains in the production state throughout the entire scheduling period, as indicated by the operating load consistently staying above the minimum threshold of 0.1. The red vertical bands indicate the optimal truck delivery schedule, with a total of six deliveries within the analyzed period. Fig. 3.b shows the corresponding hydrogen inventory level in the storage tank, which increases significantly during truck deliveries but also rises during other periods due to excess electrolyzer production.

Table 4 reports the cost components associated with the optimal plan. The overall schedule results in a total operating cost of 184,854.30 €, corresponding to a unitary hydrogen operating cost of 0.37 €/Nm^3. Electricity cost is the dominant contributor, accounting for 83% of total costs, followed by the truck delivery cost, which represents 14%. Inventory and water consumption costs are relatively small compared to other components, but they are not negligible in absolute terms. No degradation cost is incurred, as the electrolyzer operates continuously.

Fig. 4 shows the optimal results from the upper layer optimization run corresponding to 12 July. As previously mentioned, the upper layer determines the optimal scheduling of truck arrivals over a three-day prediction horizon (12–14 July). According to the optimal results, a truck is scheduled to arrive on 14 July during hour 19 (i.e., truck unloading occurs between 18 and 19), as indicated by the red vertical band. This corresponds to a period characterized by relatively low forecasted renewable energy availability and relatively high grid electricity prices, as reflected by the negative and positive normalized values, respectively, obtained by standardizing each time series using its mean and standard deviation over the scheduling horizon. Similar conditions are observed for the other truck deliveries within the scheduling horizon, indicating that these represent the circumstances

Table 3
Economic parameters.

Notation	Description	Value	Unit of measure	Reference
c^r	Unitary renewable electricity cost	0.051	€/kWh	[32]
ε^g	Electrical grid penalty cost	0.018	€/kWh	[33,34]
c^w	Unitary water consumption cost	0.004	€/Nm^3	[3,35]
h	Hydrogen holding cost factor	0.0045	€/Nm^3	[36]
c^s	Stack replacement cost factor	1,460,214	€	[10,37]
c^T	Unitary hydrogen delivery cost	0.6	€/Nm^3	[38]
c^u	Labor cost for truck unloading	30.9	€/h	[39]

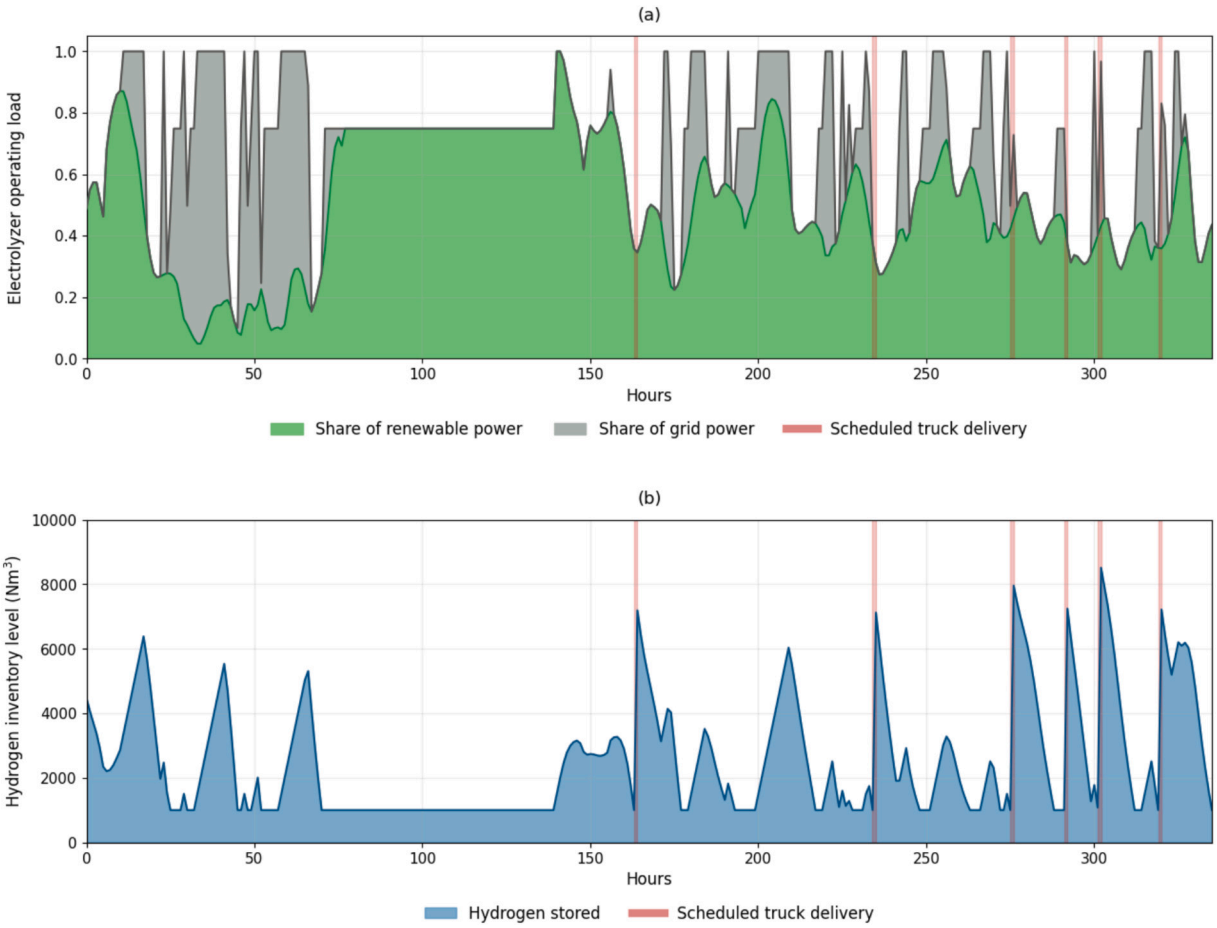

Fig. 3. Optimal hydrogen supply operations schedule for reference period (5–18 July).

Table 4
Optimal cost components for reference period (5–18 July).

Cost component	Notation	Optimal value	Share
Electricity consumption cost	EC	153,820.35 €	83%
Water consumption cost	WC	1832.00 €	1%
Hydrogen inventory cost	IC	3815.56 €	2%
Electrolyzer degradation cost	DC	0 €	0%
Truck deliveries cost	TC	25,385.40 €	14%
Total operating cost	OC	184,854.30 €	100%

under which a truck delivery becomes economically favorable. However, these conditions alone are not sufficient to trigger a delivery, as shown by the absence of truck arrivals in the final hours of 13 July. In this case, the cost of truck delivery exceeds the economic benefits derived from eliminating grid electricity consumption during the final hours of the day. This highlights the complexity of the decision-making process underlying optimal hydrogen supply operations and reinforces the need for an optimization tool to capture this complexity.

Lastly, Fig. 5 illustrates the optimal schedule for the electrolyzer's operations obtained from the lower layer optimization. The results

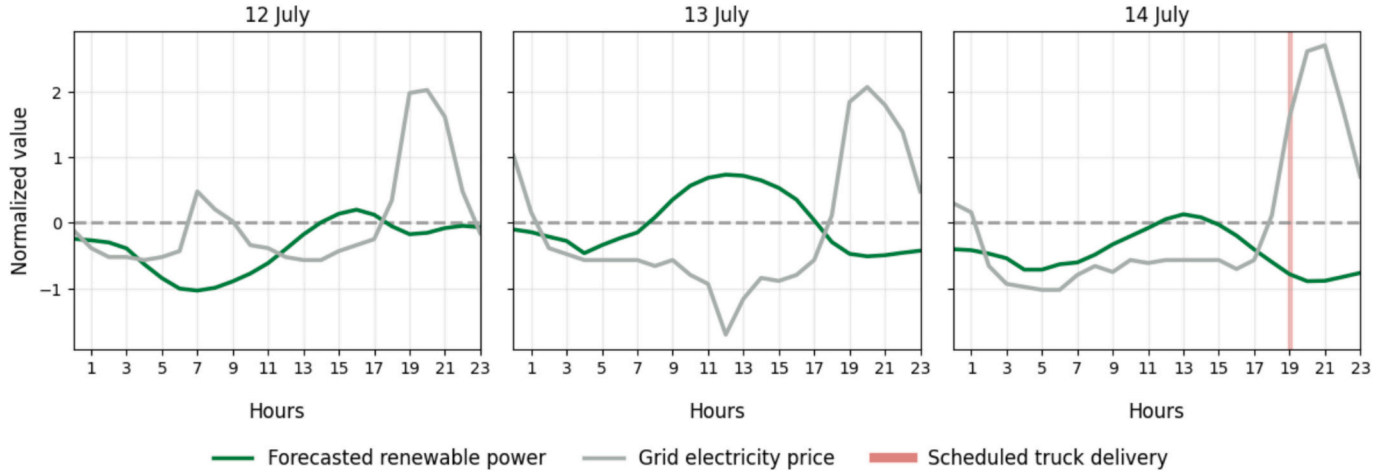

Fig. 4. Example results of the upper layer optimization (12 July).

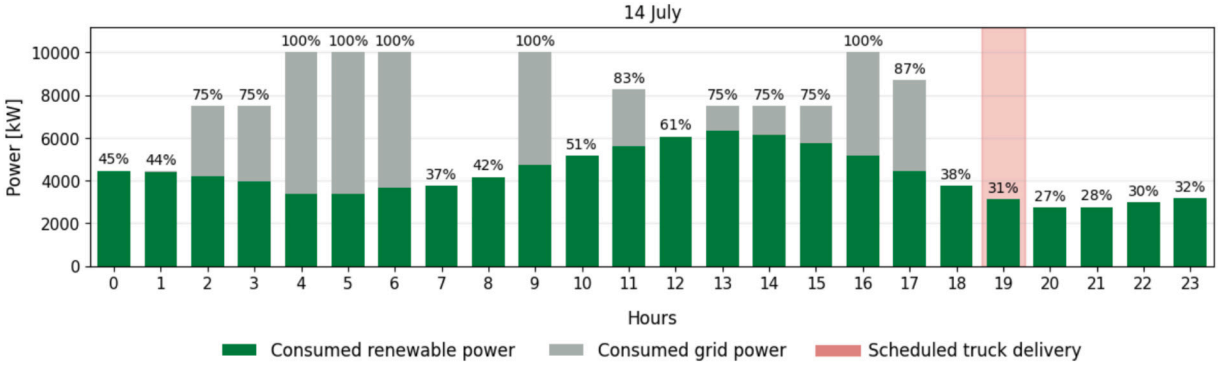

Fig. 5. Example results of the lower layer optimization (14 July).

correspond to 14 July and show, for each hour, the optimal consumption of renewable and grid power, together with the associated operating load of the electrolyzer. Because of the lower cost of renewable electricity, all available renewable power is utilized, aligning with the forecasted availability under the perfect knowledge assumption. Even when a truck delivery is scheduled, the optimal strategy is to maintain electrolyzer operation to exploit the available renewable power while storing the excess hydrogen produced or delivered for use during lower availability periods.

5.2. Optimal results for different scheduling periods under perfect knowledge

The previous results have shown that the optimal scheduling of hydrogen supply operations, including truck deliveries, as well as the electrolyzer's operating load and power mix, is strongly influenced by renewable energy availability, grid electricity prices, and the interaction between these factors. To further investigate these effects, four additional scheduling periods characterized by different average levels of renewable availability and grid prices are analyzed. Table 5 reports the selected scheduling periods, including the reference period, along with their total operating cost and corresponding unitary hydrogen operating cost. The latter is estimated from the total operating cost, accounting for the total hydrogen supplied (from both electrolyzer production and truck deliveries). Note that this cost metric does not include the impact of capital expenditures, as the scope of the study is limited to operations optimization.

The January scheduling period, labelled as HL, represents the most favorable conditions. The combination of high renewable energy availability and low grid electricity prices results in the lowest cost performance, with a unitary hydrogen operating cost of 0.27 €/Nm^3, compared to 0.37 €/Nm^3 in the reference period, labelled as MM. In contrast, the August scheduling period, labelled as LH, constitutes the least favorable scenario. Low renewable energy availability combined with high average grid electricity prices leads to the highest cost performance, with a unitary hydrogen operating cost of 0.43 €/Nm^3.

To enable a more comprehensive comparison across the different scheduling periods, additional performance indicators are introduced. The electrolyzer share is defined as the ratio between the amount of hydrogen produced by the electrolyzer and the overall hydrogen demand during the scheduling period. Similarly, the renewable share represents the contribution of renewable power to the total power consumption of the electrolyzer over the same period. To complement these performance metrics, the number of scheduled truck deliveries and the total grid power consumption over the scheduling horizon are also considered. The corresponding performance indicators for the different scheduling periods are presented in Fig. 6. Each subplot reports one performance indicator, while each cell within the inner matrix displays the corresponding indicator value for a specific scheduling period, defined by the combination of renewable energy availability and grid electricity price levels.

The favorable combination of high renewable energy availability and low grid electricity prices in the HL scenario is reflected in the corresponding performance indicators. The electrolyzer operates at its highest utilization level, resulting in a 99.21% electrolyzer share (slightly below 100% due to initial inventory assumptions) and eliminating the need for truck deliveries. The high availability of renewable power also leads to the highest renewable share across all periods, equal to 96.56%, which consequently limits total grid power consumption to 85.92 MW, despite the relatively low grid electricity prices.

In contrast, the adverse conditions of low renewable availability and high grid electricity prices in the LH period are reflected by the significant reduction in electrolyzer share to 58.93%. Due to high grid electricity prices, the electrolyzer operates mainly on limited renewable power, resulting in a relatively high renewable share, equal to 89.01%. The reduced on-site hydrogen production is compensated by increased external supply, leading to the highest number of scheduled truck deliveries, equal to 29. Interestingly, the optimal solution for this scheduling period includes a hot start-up, which reduces the maximum hydrogen production rate at full load to 2003.61 Nm^3/h, compared to 2003.71 Nm^3/h under nominal efficiency levels. When the degradation effect is excluded from the model, the optimal solution involves switching the electrolyzer off in different hours (idle state), resulting in three cold start-up transitions. This behavior is driven by the cost of remaining on standby and by the model's lack of visibility regarding long-term degradation effects. However, this strategy ultimately results in a larger efficiency loss, lowering the hydrogen production rate at full load to 2000.56 Nm^3/h. These findings underscore the importance of explicitly incorporating degradation into the model, as omitting this effect encourages decisions that achieve short-term cost savings but ultimately accelerate performance deterioration and reduce long-term operational efficiency.

Table 5
Optimal hydrogen supply operations cost performance under different scheduling periods.

Period	Average renewable availability	Average grid price	Label	OC [€]	Unitary hydrogen operating cost [€/Nm^3]
17–30 January	High	Low	HL	135,842.87	0.27
16–29 May	Low	Low	LL	205,529.24	0.41
10–23 August	Low	High	LH	217,212.58	0.43
4–17 November	High	High	HH	161,594.18	0.32
5–18 July (Reference)	Medium	Medium	MM	184,854.30	0.37

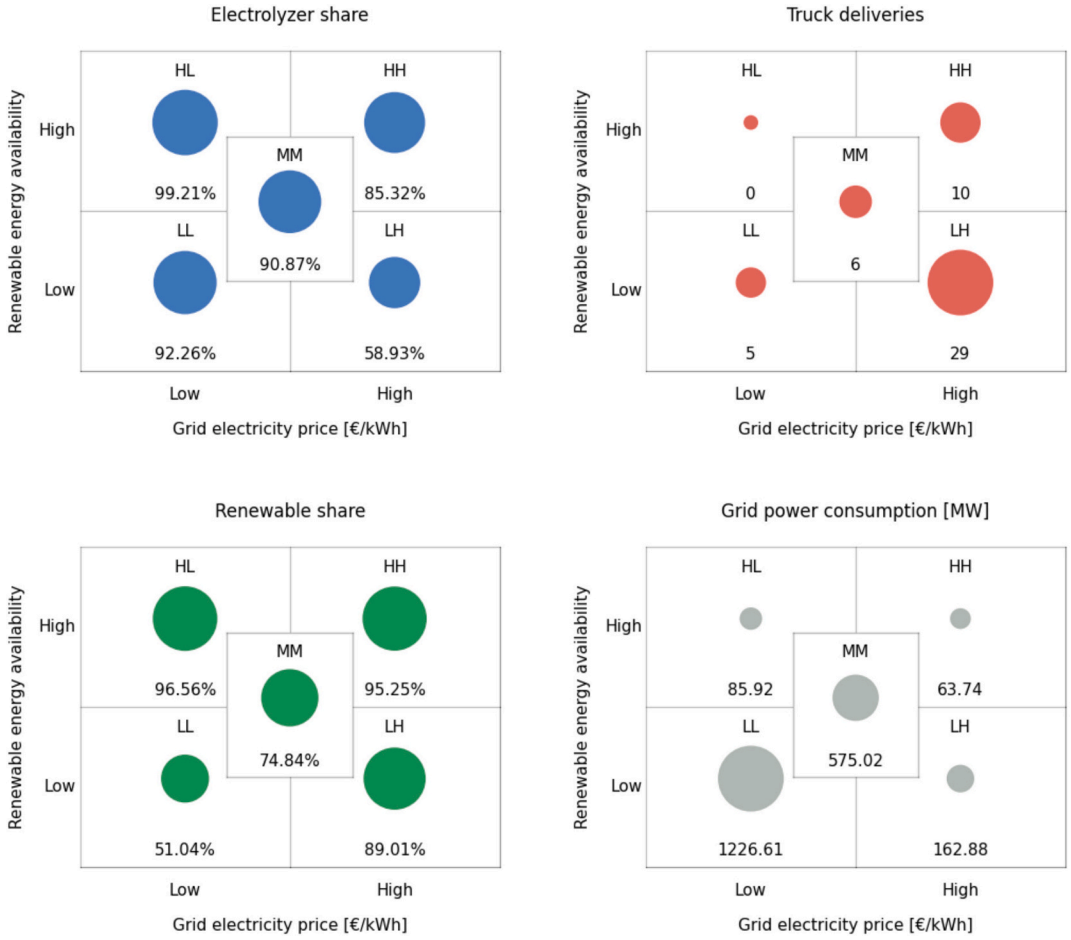

Fig. 6. Optimal hydrogen supply operations performance under different scheduling periods, characterized by varying renewable energy availability and grid price levels. Each subplot presents a specific performance indicator, while the inner matrix shows the corresponding outcomes for different combinations of renewable availability and grid price levels.

The moderate external conditions characterizing the reference period, labelled as MM, lead to intermediate values for electrolyzer share and truck deliveries, equal to 90.87% and 6, respectively. Because neither renewable availability nor grid prices are particularly high, the renewable share decreases to 74.84%, resulting in a higher reliance on grid electricity and a total grid power consumption of 575.02 MW.

Periods with comparable grid electricity prices can be contrasted to better understand the role of renewable energy availability. For instance, while both LL and HL periods are characterized by low grid prices, the lower renewable availability in LL significantly affects the optimal power mix, leading to the lowest renewable share and the highest grid power consumption, equal to 51.04% and 1226.61 MW, respectively. Nevertheless, the low grid price makes it possible to maintain a high electrolyzer share, equal to 92.26%, even though five truck deliveries are scheduled.

A comparison can also be made between scheduling periods with similar renewable energy availability levels and different grid energy prices. Both LL and LH periods exhibit low renewable availability, but lower grid prices in LL make it optimal to use grid electricity extensively, resulting in the highest grid power consumption of 1226.61 MW. As a result, the electrolyzer share remains high at 92.26%, and only five truck deliveries are scheduled. In contrast, the higher grid electricity prices in LH make grid use unfavorable, causing the electrolyzer to rely primarily on renewables. As a consequence, the electrolyzer share decreases to 51.04%, and truck deliveries become the most cost-effective backup option.

The results across the different scheduling periods highlight that no single backup option is universally optimal. Instead, the cost-effective solution depends on external factors such as renewable energy availability and grid electricity prices. This finding underscores the value of integrating both grid electricity purchases and external hydrogen deliveries within the same optimization framework. By enabling the simultaneous modeling of both backup options through the proposed multi-timescale structure, the framework allows the selection of the most cost-effective backup option or the optimal combination of both alternatives under varying external conditions.

5.3. *Trade-off analysis of backup operational strategies*

The previous analysis showed that, under comparable levels of renewable energy availability, a clear trade-off exists between alternative backup options used to ensure hydrogen demand fulfillment. To further investigate this relationship, a sensitivity analysis is performed on both the penalty cost associated with grid electricity purchases and the cost of externally delivered hydrogen. Given that these analyses lead to similar but opposite conclusions, only the results related to the cost of externally delivered hydrogen are presented here, while the sensitivity analysis on the grid electricity penalty cost is reported in Appendix A.

Fig. 7 reports the results obtained when varying the unitary cost of externally delivered hydrogen across the different scheduling periods. While the baseline cost is set to 0.6 €/Nm^3, the sensitivity analysis explores a range from 0.4 to 0.8 €/Nm^3. As illustrated in Fig. 7.a, increasing the hydrogen delivery cost leads to a reduction in the number of truck deliveries. To continue fulfilling the hydrogen demand, the system compensates by increasing grid electricity consumption, as depicted in Fig. 7.b. Fig. 7.c shows that the total operating cost increases with higher hydrogen delivery costs; however, the marginal increase

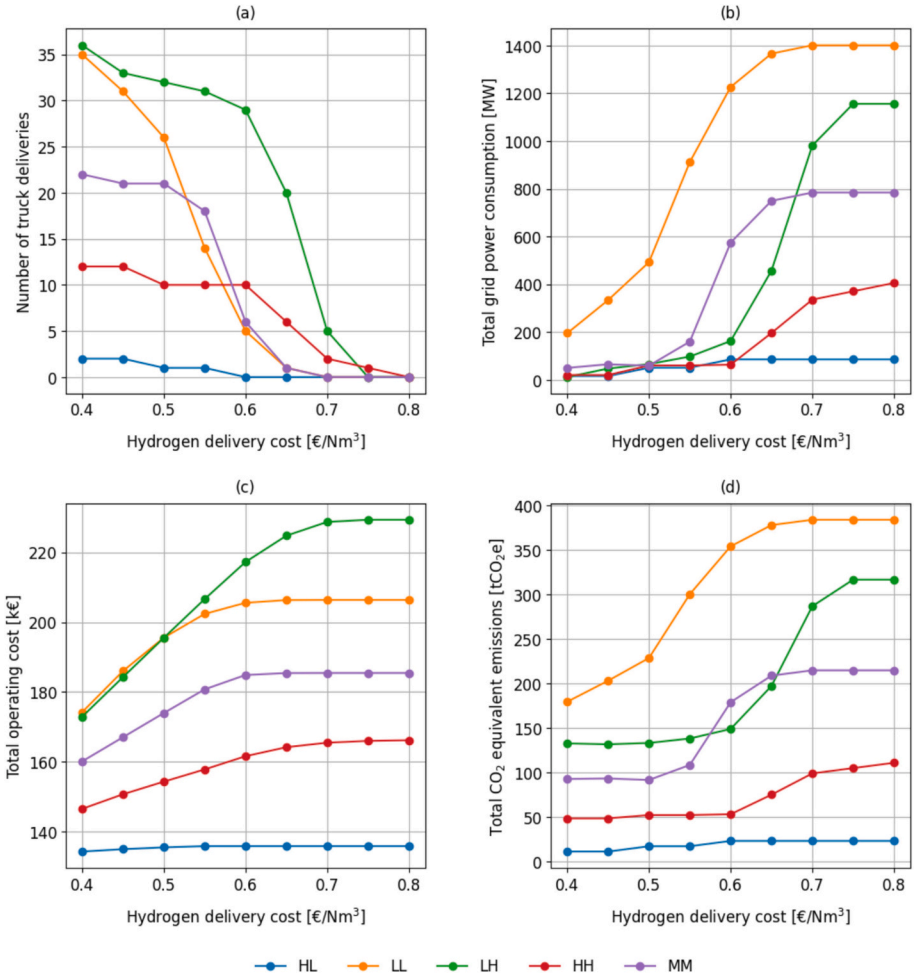

Fig. 7. Effect of varying hydrogen delivery cost on number of truck deliveries (a), total grid power consumption (b), total operating cost (c), and total CO_2 equivalent emissions (d) across different scheduling periods.

becomes smaller at higher delivery cost levels due to the progressive elimination of truck deliveries. Interestingly, Fig. 7.a also shows that relying solely on grid electricity as a backup option is economically preferable only when the hydrogen delivery cost is equal to or exceeds 0.8 €/Nm^3, as indicated by the absence of truck deliveries in the corresponding optimal solutions. For lower hydrogen delivery costs, complementing grid usage with truck deliveries remains economically advantageous, particularly for periods characterized by higher electricity prices (i.e., LH and HH). Since the two backup options exhibit substantially different environmental performance, and emission reduction represents the primary objective of the hydrogen transition, the impact of varying the unitary cost of externally delivered hydrogen on total CO_2 equivalent emissions is explicitly quantified and illustrated in Fig. 7.d. Grid-related emissions are estimated using the average carbon intensity of the electrical grid in the analyzed case study. For external hydrogen deliveries, the assessment includes both the indirect emissions associated with green hydrogen production and the emissions resulting from fuel consumption during transportation. The results show that an increase in the hydrogen delivery cost, and the resulting reduction in scheduled truck deliveries, leads to higher CO_2 equivalent emissions. These results suggest that overall emissions are primarily driven by increased reliance on grid electricity consumption. This outcome is explained by the relatively high carbon intensity of the electrical grid in the analyzed case study, combined with the assumption that externally supplied hydrogen is produced from renewable sources. It is important to note that different conclusions may emerge under alternative grid carbon intensities or under different assumptions regarding the production pathway of externally supplied hydrogen.

5.4. *Robustness to forecast inaccuracies in renewable energy availability*

This section investigates how different levels of forecast accuracy affect optimal results. While the analysis focuses on forecast inaccuracies in renewable energy availability, additional experiments conducted for the reference scheduling period, considering electricity price forecast errors, resulted in similar cost impacts and robustness trends.

The analysis is presented in detail for the baseline scheduling period in July, while the results for all the scheduling periods considered in Table 5 are provided in Appendix B. The actual renewable energy availability values are kept identical to those in the perfect knowledge case (representative year 2014), and the baseline values of all other input parameters are maintained to isolate the effect of forecast accuracy. Synthetic forecasts are generated by smoothing the actual data and adding correlated Gaussian noise, while ensuring that all values remain within the [0,1] range. The smoothing determines the extent to which the forecast captures short-term fluctuations, while the Gaussian noise represents forecast errors and simulates the level of uncertainty in the forecast. The noise is made temporally correlated to reproduce the temporal persistence typically observed in wind power availability. Because of the stochastic noise component, five different random seeds are used to generate forecasts for each scenario.

Table 6 summarizes the parameters adopted for synthetic forecast generation and reports the average performance metrics of the forecasts relative to the actual data across seeds. Forecast accuracy decreases

Table 6
Synthetic forecast generation parameters and average performance metrics across different seeds for reference period (5–18 July).

Forecast Scenario	Smoothing window	Gaussian noise standard deviation	Correlation noise	Average MAE	Average MAPE	Average R^2
High accuracy	3	0.1	0.98	0.0201	14.13%	0.9577
Medium accuracy	6	0.2	0.98	0.0412	28.48%	0.8245
Low accuracy	12	0.3	0.98	0.0637	42.53%	0.5825

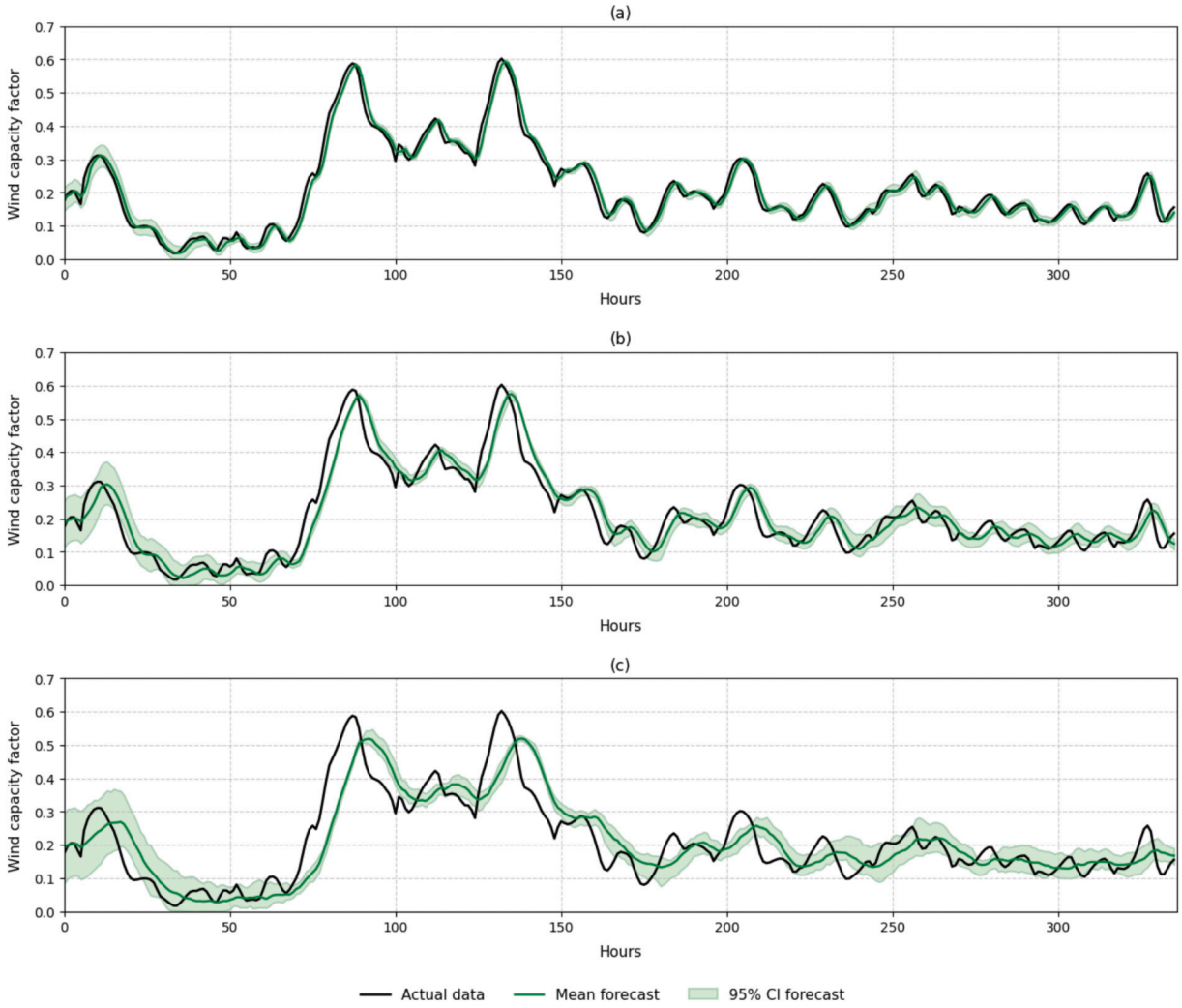

Fig. 8. Mean and 95% confidence interval across seeds for forecast scenarios with high (a), medium (b) and low (c) accuracy, compared with actual data for reference period (5–18 July).

across the scenarios presented in the table. This decreasing accuracy trend is further illustrated in Fig. 8, which shows the mean forecast values along with the corresponding 95% confidence interval (CI).

Fig. 9 illustrates the model's behavior under the rolling horizon approach when the forecasts do not match the actual renewable energy availability. The results refer to a forecast scenario with low accuracy and are obtained from three consecutive iterations of the lower layer optimization, corresponding to hours 235–237 of the reference scheduling horizon (5–18 July). The red rectangle highlights the current hour, for which the actual renewable energy availability is updated relative to the forecasted value and the optimal operations are implemented. All preceding hours correspond to operational decisions that have already been executed and can no longer be modified. All other hours within the 24-h prediction horizon, including the current ones, can be re-optimized based on the observed renewable energy availability. This is evident in the figure, where the operational decisions for the current hour and the subsequent ones (e.g., hours 240 and 241) are updated accordingly in terms of the electrolyzer's operating load and power mix.

While the optimal decisions concerning the electrolyzer's operations can be re-optimized on an hourly basis in accordance with the observed renewable energy availability, the same does not apply to truck deliveries, whose scheduling depends solely on the available forecasts. As a result, the truck delivery schedule, in terms of both the number of deliveries and their timing, is influenced by the forecast accuracy. Fig. 10 illustrates the scheduled truck deliveries obtained under different forecast accuracy scenarios (across multiple seeds), compared with the optimal delivery schedule under perfect knowledge, highlighted in red. As shown in Fig. 10.c, reduced forecast accuracy leads to larger and more dispersed deviations from the optimal truck delivery schedule obtained under the perfect knowledge scenario over the scheduling horizon.

Nevertheless, the overall cost performance obtained under the proposed optimization framework is not strongly affected by forecast accuracy, as shown in Table 7. Even in a scenario with very poor forecast

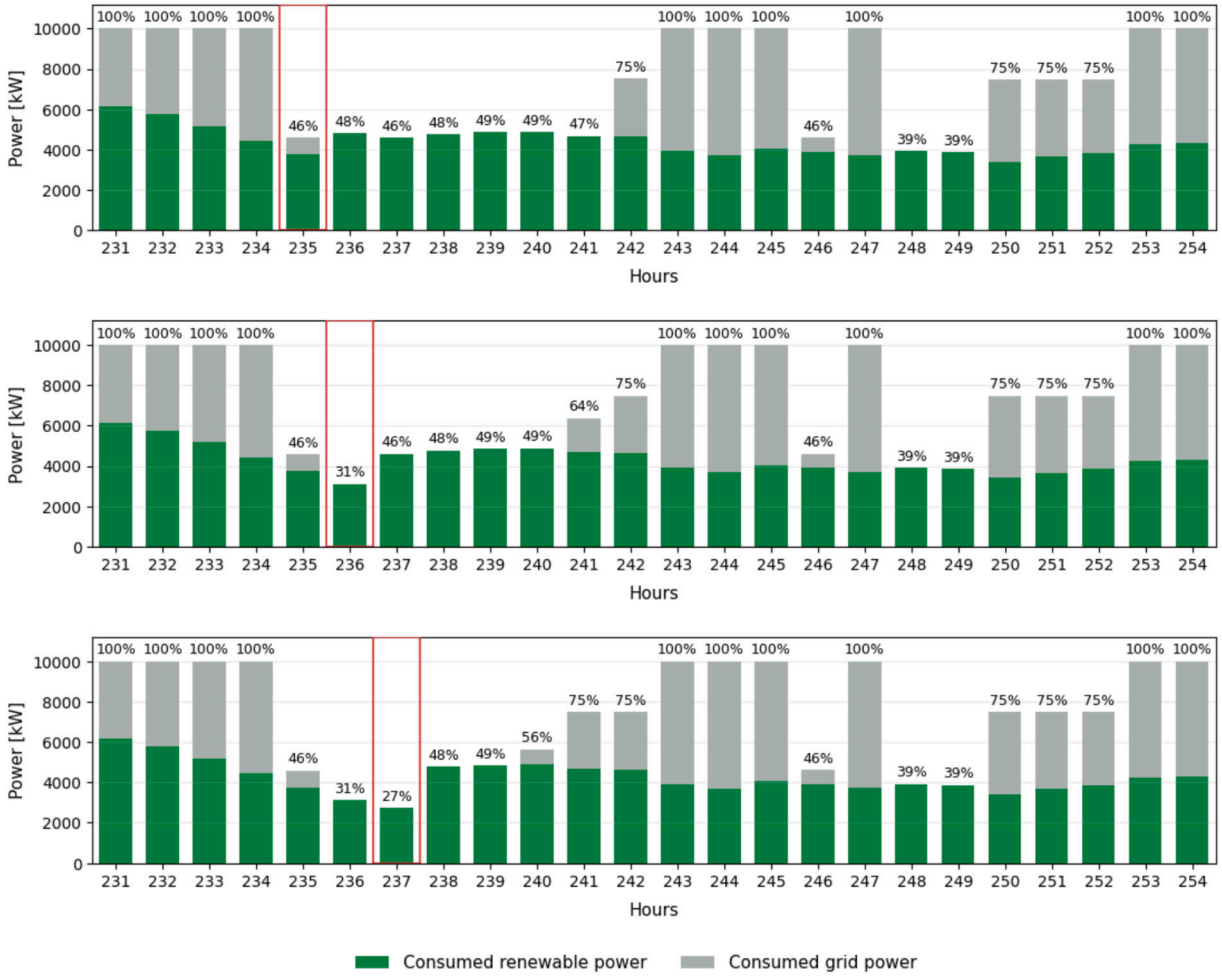

Fig. 9. Model's behavior under the rolling horizon approach over three consecutive hours of operation during reference period (5–18 July).

performance, the maximum percentage increase in total operating cost over the perfect knowledge case is only 2.80%, demonstrating the robustness of the modeling approach to forecast accuracy.

When considering the results across the different scheduling periods, a maximum average increase of 2.47% in total operating cost relative to perfect knowledge is observed (Appendix B). These results highlight the effectiveness of integrating a rolling horizon approach within the proposed multi-timescale optimization framework, as re-optimizing the electrolyzer's operational decisions in response to realized renewable energy availability mitigates the impact of forecast errors.

In addition to cost performance, the computational performance of the proposed optimization framework under different forecast accuracy levels is assessed. The average and maximum computational times per rolling horizon iteration for both the upper and lower layers are reported in Table 8. The results confirm the practical applicability of the proposed approach for online implementation, as the computational times remain significantly lower than the length of the corresponding control horizons.

5.5. Comparative analysis with static optimization

Under a static optimization approach, all decisions are optimized at the start of the scheduling horizon, assuming complete foresight over the entire period, and no re-optimization takes place when new information becomes available. Accordingly, the MINLP formulation presented in Section 3.3 is solved once over the entire scheduling horizon. Depending on the scenario analyzed, the input values for renewable energy availability correspond either to the actual data or to the forecasted values presented in the previous section.

Because of the mismatch between forecasted and observed renewable energy availability, an optimal operations schedule obtained under static optimization may become infeasible during implementation. To derive a feasible operational plan from the static schedule, while keeping deviations from the optimized schedule to a minimum, it is assumed that any shortfall in renewable energy availability relative to the forecast can be compensated by additional grid consumption. This assumption preserves the optimal plan in terms of the electrolyzer's operating load, truck deliveries, and hydrogen storage levels, while ensuring feasibility under the actual renewable energy availability.

Fig. 11 compares the results obtained across different seeds when either a static optimization approach or a rolling horizon approach is applied under different forecast accuracy scenarios. Under the perfect knowledge case, the static optimization outperforms the rolling horizon approach, as it benefits from full foresight over the entire scheduling period when optimizing decisions. However, once deviations arise between forecasted and actual renewable energy availability, the static approach begins to underperform the rolling horizon approach, with performance worsening as forecast accuracy decreases. The static optimization approach also shows much higher variability across seeds, confirming the greater robustness of the rolling horizon approach under imperfect knowledge. These results show that in a practical setting, where forecasts are inherently imperfect, the rolling horizon approach is better suited to deal with the uncertainty related to renewable energy availability.

Table 9 confirms these findings by reporting the average optimal cost performance obtained across seeds under the different forecast accuracy

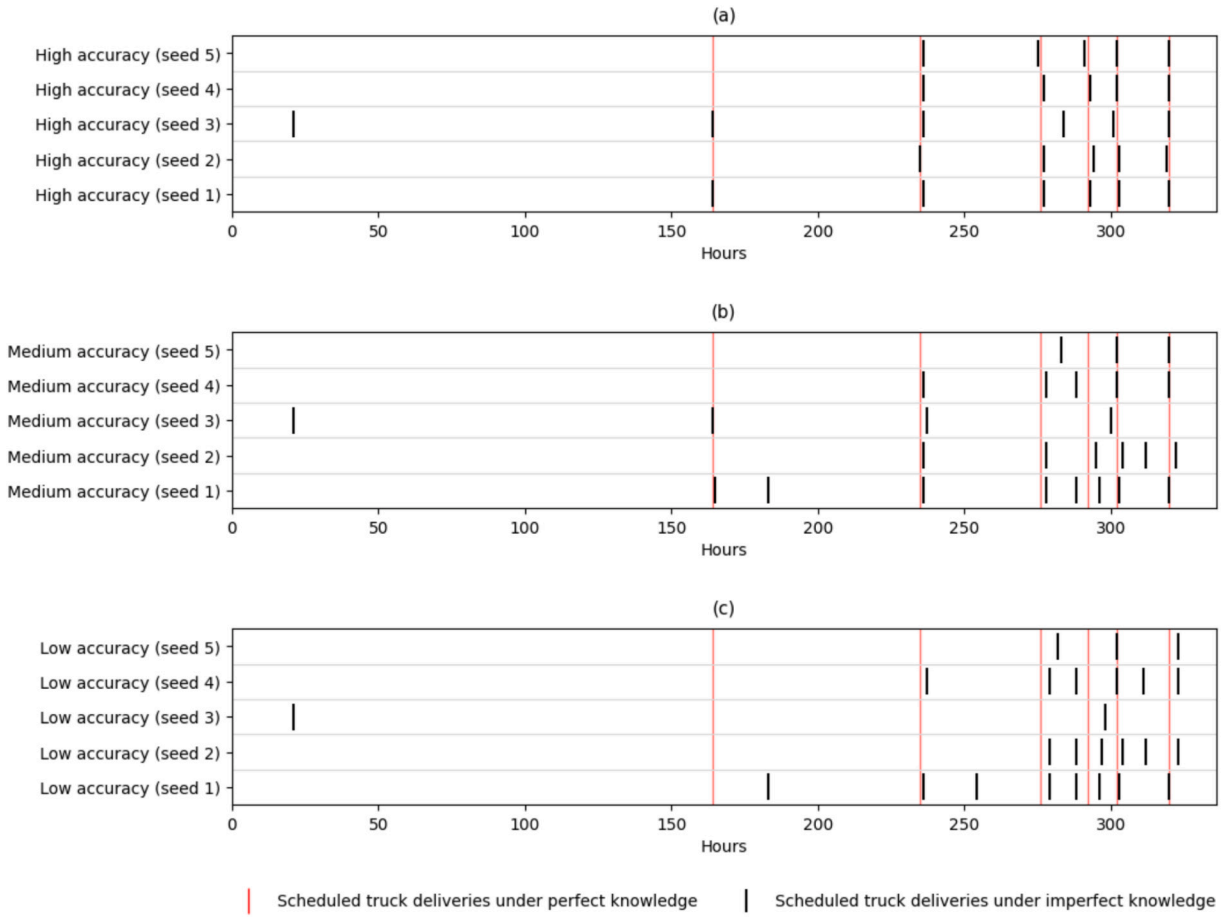

Fig. 10. Scheduled truck deliveries under forecast scenarios with high (a), medium (b), and low (c) accuracy (black), compared with the optimal truck delivery schedule obtained under perfect knowledge (red), over the reference period (5–18 July). (For interpretation of the references to colour in this figure legend, the reader is referred to the web version of this article.)

Table 7
Effect of forecast accuracy on optimal cost performance under the rolling horizon approach for reference period (5–18 July).

Forecast scenario	Average OC [€]	Average unitary hydrogen operating cost [€/Nm^3]	Percentage variation
Perfect knowledge	184,854.30	0.367	–
High accuracy	185,756.98	0.369	+ 0.49%
Medium accuracy	188,046.60	0.373	+ 1.73%
Low accuracy	190,032.01	0.377	+ 2.80%

scenarios for the static optimization approach. Even if a 0.86% reduction in total operating cost can be achieved with a static optimization approach under the perfect knowledge case, the rolling horizon approach leads to average cost reductions ranging between 1.83% and 6.24% under imperfect knowledge. Moreover, while poor forecast performance increases the total operating cost by 2.80% relative to the perfect knowledge case when using the rolling horizon approach (Table 7), the same forecast conditions result in an average increase of 10.17% under static optimization, which is more than three times higher.

When considering the results obtained by implementing a static optimization across all scheduling periods (Appendix C), the average maximum increase over perfect knowledge is 8.17%, which remains more than three times higher than that observed with the rolling horizon approach. Additionally, under perfect knowledge, static optimization results in an average cost reduction of 0.82% compared to the rolling horizon. However, under imperfect knowledge, the maximum average increase in total cost relative to the rolling horizon approach reaches 4.15%, confirming the superior robustness of the rolling horizon approach to forecast inaccuracies.

6. Conclusions

A dynamic scheduling optimization framework for hydrogen supply operations is proposed in this paper. The framework incorporates a multi-timescale structure that enables the coordinated management of

Table 8
Computational time performance per rolling horizon iteration in upper and lower layers for reference period (5–18 July).

Computational time performance	Perfect Knowledge		Imperfect Knowledge (High accuracy)		Imperfect Knowledge (Medium accuracy)		Imperfect Knowledge (Low accuracy)	
	Upper layer	Lower layer	Upper layer	Lower layer	Upper layer	Lower layer	Upper layer	Lower layer
Average (s)	1.143	0.267	1.601	0.326	1.601	0.322	1.365	0.273
Maximum (s)	1.536	0.504	3.161	1.551	3.609	1.201	2.112	1.2

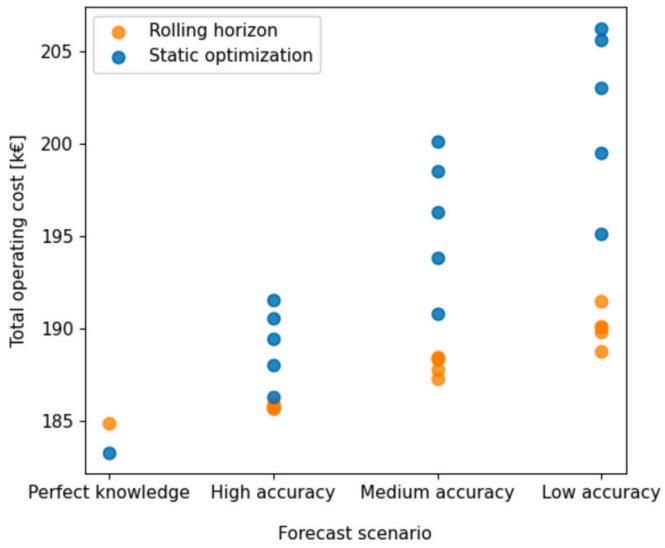

Fig. 11. Static and rolling horizon model performance under different forecast quality scenarios for reference period (5–18 July).

electrolyzer-based hydrogen production and external hydrogen deliveries via truck transport, which serve as an alternative backup option to grid electricity purchases to ensure the continuous fulfillment of hydrogen demand from industrial furnaces. The adoption of a rolling horizon approach eliminates the need for long-term forecasts, which are often difficult to obtain, and allows reactive scheduling of electrolyzer operations (operational state, load, and power mix) as new observations of renewable energy availability become available. The main findings can be summarized as follows:

- The overall economic performance and the resulting optimal hydrogen supply operations are strongly dependent on renewable energy availability and grid electricity prices. A variation of approximately 60% in total operating cost is observed between the best conditions (high renewable energy availability and low electricity prices) and the worst (low renewable energy availability and high electricity prices), resulting in a unitary hydrogen operating cost ranging between 0.27 and 0.43 €/Nm^3.
- A clear trade-off exists between grid electricity purchases and external hydrogen deliveries when used as backup options to ensure continuous fulfillment of hydrogen demand. In contexts with carbon-intensive grids, projected increases in carbon taxation may make external hydrogen deliveries more economically favorable for covering shortfalls in renewable energy availability. Under current carbon taxation levels and limited renewable energy availability, relying solely on grid electricity results in the most attractive backup option across different scheduling periods only when the external hydrogen delivery cost is equal to or above 0.8 €/Nm^3.
- While forecast inaccuracies significantly affect external delivery decisions, which rely solely on forecast information, the reactive scheduling of electrolyzer operations based on newly observed renewable energy availability through a rolling horizon approach limits the increase in total operating cost across different scheduling periods to only 2.47%, even under very poor forecast accuracy. In contrast, relying on static optimization can raise total operating costs by up to 8.17%, highlighting the higher robustness of the rolling horizon approach to forecast inaccuracies.
- Although static optimization improves economic performance across different scheduling periods by 0.82% when perfect knowledge of future renewable energy availability is assumed, the rolling horizon approach can reduce total operating cost by up to 4.15% compared to static optimization under imperfect forecasts.

Despite these contributions, some limitations remain and suggest promising directions for future research. The use of synthetic forecasts does not fully replicate the statistical characteristics of real wind capacity factor forecast errors. However, this approach enables a controlled evaluation of the robustness of the proposed framework under varying levels of forecast accuracy. The use of real historical forecast datasets as an additional robustness assessment represents a valuable extension of the present study. Nevertheless, its implementation would require overcoming practical challenges, such as differences in temporal resolution and forecast horizon length in publicly available historical forecast data. Future research may also extend the proposed framework by refining the modeling of electrolyzer operations. This includes representing efficiency as a function of operating load and modeling stack degradation under additional operating conditions beyond start-up transitions. Furthermore, incorporating real-time weather data together with forecasting techniques would reduce or eliminate reliance on externally provided forecasts and advance the proposed optimization framework toward Digital Twin-based hydrogen production operations.

Declaration of generative AI and AI-assisted technologies in the manuscript preparation process

During the preparation of this work the authors used GPT-5 in order to improve language clarity, readability, and grammar across all sections of the manuscript. After using this tool/service, the authors reviewed and edited the content as needed and take full responsibility for the content of the published article.

CRediT authorship contribution statement

Giulia Fede: Writing – review & editing, Writing – original draft, Visualization, Validation, Software, Methodology, Investigation, Formal analysis, Conceptualization. **Fabio Sgarbossa:** Writing – review & editing, Supervision, Project administration, Funding acquisition, Conceptualization. **Daniel F. Silva:** Writing – review & editing, Supervision, Methodology, Conceptualization.

Funding sources

This work received funding from the European Union's Horizon Europe research and innovation program under the Grant Agreement No. 101092153. Views and opinions expressed are however those of the authors only and do not necessarily reflect those of the European Union or European Health and Digital Executive Agency. Neither the European Union nor the granting authority can be held responsible for them.

Table 9
Effect of forecast accuracy on optimal cost performance under the static optimization approach for reference period (5–18 July).

Forecast scenario	Average OC [€]	Average unitary hydrogen operating cost [€/Nm^3]	Percentage variation over rolling horizon	Percentage variation over perfect knowledge
Perfect knowledge	183,265.36	0.364	- 0.86%	–
High accuracy	189,151.70	0.375	+ 1.83%	+ 3.21%
Medium accuracy	195,895.75	0.389	+ 4.17%	+ 6.89%
Low accuracy	201,898.32	0.401	+ 6.24%	+ 10.17%

Declaration of competing interest

The authors declare that they have no known competing financial interests or personal relationships that could have appeared to influence the work reported in this paper.

Appendix A. Sensitivity analysis on grid penalty cost

Fig. A.1. presents the results obtained from varying the penalty cost associated with grid usage, reflecting changes in the carbon allowance price, across the different scheduling periods. The baseline grid electricity penalty is 0.018 €/kWh, corresponding to an average carbon allowance price equal to 0.067 €/kgCO_2 and an average grid carbon intensity of 0.274 kgCO_2e/kWh. The sensitivity analysis considers grid electricity penalty values ranging from 0.008 to 0.028 €/kWh, equivalent to carbon allowance prices between 0.029 and 0.102 €/kgCO_2.

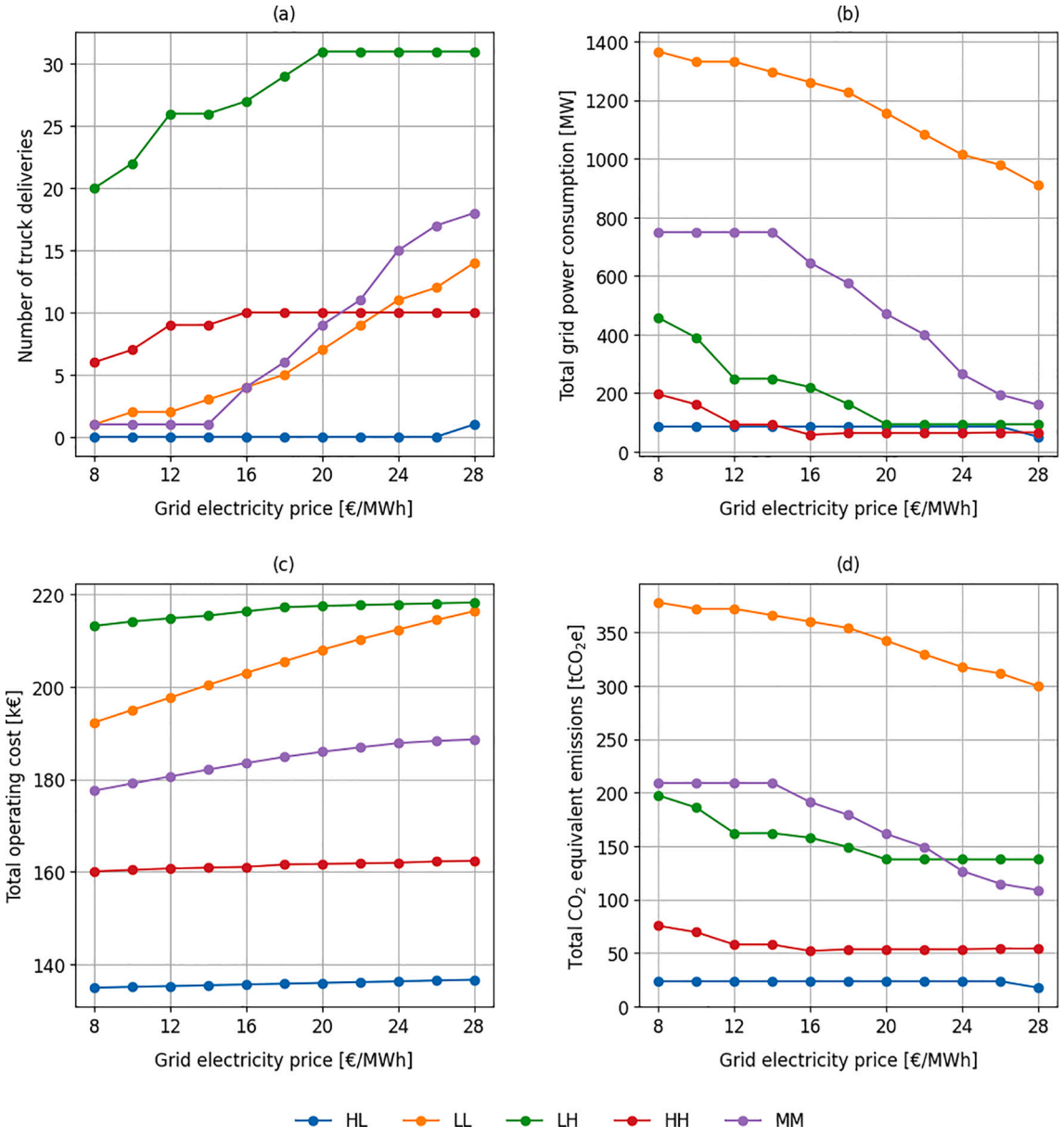

Fig. A.1. Effect of varying grid electricity penalty on number of truck deliveries (a), total grid power consumption (b), total operating cost (c), and total CO_2 equivalent emissions (d) across different scheduling periods.

As the grid penalty increases, the number of truck deliveries rises, while total grid power consumption decreases, as shown in Fig. A.1.a and Fig. A.1.b, respectively. This reflects a progressive shift from grid electricity purchases toward external hydrogen deliveries as the preferred backup option, driven by the higher penalized cost associated with grid consumption. The increase in the grid penalty also results in higher total operating costs, as illustrated in Fig. A.1.c, although the relationship is not linear. In particular, Fig. A.1.c shows that at higher grid penalty values, the marginal increase in total cost becomes smaller (especially evident for the scheduling period MM). This occurs because once grid consumption has been significantly reduced, further increases in the grid penalty apply only to a small remaining share of grid electricity. As a result, the impact of a higher grid penalty on total operating cost becomes progressively smaller. Finally, Fig. A.1.d presents the trend in total CO_2 equivalent emissions. Emissions decrease as the grid penalty increases, primarily due to the reduction in grid power consumption.

Appendix B. Robustness to forecast inaccuracies in renewable energy availability (extended results)

See Table A.1.

Table A.1
Effect of forecast accuracy on optimal cost performance under the rolling horizon approach for different scheduling periods.

Scheduling period	Forecast scenario	Average MAPE	Average R^2	Average OC [€]	Average unitary hydrogen operating cost [€/Nm^3]	Percentage variation
17–30 January	Perfect knowledge	–	–	135,842.87	0.270	–
	High accuracy	5.58%	0.9660	136,496.95	0.271	+ 0.48%
	Medium accuracy	11.61%	0.8586	137,322.58	0.272	+ 1.09%
	Low accuracy	17.80%	0.6627	138,379.04	0.275	+ 1.87%
16–29 May	Perfect knowledge	–	–	205,529.24	0.408	–
	High accuracy	12.62%	0.9195	205,855.28	0.408	+ 0.16%
	Medium accuracy	24.92%	0.6960	206,479.64	0.410	+ 0.46%
	Low accuracy	37.70%	0.3436	206,804.89	0.410	+ 0.62%
10–23 August	Perfect knowledge	–	–	217,212.58	0.431	–
	High accuracy	16.51%	0.9342	218,290.21	0.433	+ 0.50%
	Medium accuracy	33.45%	0.7162	223,495.33	0.443	+ 2.89%
	Low accuracy	46.61%	0.4298	228,292.21	0.453	+ 5.10%
4–17 November	Perfect knowledge	–	–	161,594.18	0.321	–
	High accuracy	8.05%	0.9695	163,086.75	0.324	+ 0.92%
	Medium accuracy	16.69%	0.8804	165,480.82	0.328	+ 2.41%
	Low accuracy	28.92%	0.7210	168,991.98	0.335	+ 4.58%
5–18 July (Reference)	Perfect knowledge	–	–	184,854.30	0.367	–
	High accuracy	14.13%	0.9577	185,756.98	0.369	+ 0.49%
	Medium accuracy	28.48%	0.8245	188,046.60	0.373	+ 1.73%
	Low accuracy	42.53%	0.5825	190,032.01	0.377	+ 2.80%
Average	Perfect knowledge	–	–	–	–	–
	High accuracy	11.38%	0.9494	–	–	+ 0.51%
	Medium accuracy	23.03%	0.7951	–	–	+ 1.42%
	Low accuracy	39.32%	0.5479	–	–	+ 2.47%

Appendix C. Comparative analysis with static optimization (extended results)

See Table A.2.

Table A.2
Effect of forecast accuracy on optimal cost performance under the static optimization approach for different scheduling periods.

Scheduling period	Forecast scenario	Average OC [€]	Average unitary hydrogen operating cost [€/Nm^3]	Percentage variation over rolling horizon	Percentage variation over perfect knowledge
17–30 January	Perfect knowledge	135,193.10	0.268	- 0.48%	–
	High accuracy	136,525.82	0.271	+ 0.02%	+ 0.99%
	Medium accuracy	138,088.86	0.274	+ 0.56%	+ 2.14%
	Low accuracy	139,944.09	0.278	+ 1.13%	+ 3.51%
16–29 May	Perfect knowledge	205,441.58	0.408	- 0.04%	–
	High accuracy	210,167.37	0.417	+ 2.10%	+ 2.3%
	Medium accuracy	214,030.42	0.427	+ 3.66%	+ 4.18%
	Low accuracy	217,923.35	0.432	+ 5.38%	+ 6.08%
10–23 August*	Perfect knowledge	215,461.44	0.428	- 0.81%	–
	High accuracy	223,602.38	0.444	+ 2.43%	+ 3.78%
	Medium accuracy	233,469.96	0.463	+ 4.46%	+ 8.36%
	Low accuracy	240,438.29	0.477	+ 5.33%	+ 11.59%
4–17 November	Perfect knowledge	158,466.64	0.314	−1.94%	–
	High accuracy	163,019.22	0.323	−0.04%	+ 2.87%
	Medium accuracy	167,826.13	0.333	+ 1.42%	+ 5.91%
	Low accuracy	173,524.19	0.344	+ 2.68%	+ 9.50%
5–18 July (Reference)	Perfect knowledge	183,265.36	0.364	- 0.86%	–
	High accuracy	189,151.70	0.375	+ 1.83%	+ 3.21%
	Medium accuracy	195,895.75	0.389	+ 4.17%	+ 6.89%
	Low accuracy	201,898.32	0.401	+ 6.24%	+ 10.17%
Average	Perfect knowledge	–	–	- 0.82%	–
	High accuracy	–	–	+ 1.27%	+ 2.63%
	Medium accuracy	–	–	+ 2.85%	+ 5.50%
	Low accuracy	–	–	+ 4.15%	+ 8.17%

* For this scheduling period, a time limit of 10 min was imposed to solve the static optimization problem due to its higher computational effort compared to the rolling horizon approach. The resulting solutions exhibit a maximum and average relative optimality gap of 0.37% and 0.14%, respectively.

Data availability

Data will be made available on request.

References

[1] International energy agency (IEA). Energy systems - Industry 2023. https://www.iea.org/energy-system/industry.

[2] Bruyn SD, Jongsma C, Kampman B, Görlach B. Jan-Erik Thie. Energy-intensive industries: Challenges and opportunities in energy transition. 2020. https://doi.org/10.13140/RG.2.2.34247.52649.

[3] Ademollo A, Mati A, Pagliai M, Carcasci C. Exploring the role of hydrogen in decarbonizing energy-intensive industries: a techno-economic analysis of a solid oxide fuel cell cogeneration system. J Clean Prod 2024;469:143254. https://doi.org/10.1016/j.jclepro.2024.143254.

[4] Marocco P, Gandiglio M, Audisio D, Santarelli M. Assessment of the role of hydrogen to produce high-temperature heat in the steel industry. J Clean Prod 2023;388:135969. https://doi.org/10.1016/j.jclepro.2023.135969.

[5] Lu X, Du B, Zhou S, Zhu W, Li Y, Yang Y, et al. Optimization of power allocation for wind-hydrogen system multi-stack PEM water electrolyzer considering degradation conditions. Int J Hydrogen Energy 2023;48:5850–72. https://doi.org/10.1016/j.ijhydene.2022.11.092.

[6] Bak Y, Ryu H, Choi G, Lee D, Lee JM. Optimization of operational strategies for industrial applications of solar-based green hydrogen. Appl Energy 2025;377:124693. https://doi.org/10.1016/j.apenergy.2024.124693.

[7] Superchi F, Mati A, Carcasci C, Bianchini A. Techno-economic analysis of wind-powered green hydrogen production to facilitate the decarbonization of hard-to-abate sectors: a case study on steelmaking. Appl Energy 2023;342:121198. https://doi.org/10.1016/j.apenergy.2023.121198.

[8] Barigozzi G, Brumana G, Franchini G, Ghirardi E, Ravelli S. Techno-economic assessment of green hydrogen production for steady supply to industrial users. Int J Hydrogen Energy 2024;59:125–35. https://doi.org/10.1016/j.ijhydene.2024.02.033.

[9] Guo H, Zhang C, Wang J, Wu Z, Wang T, Wang P, et al. Design and operation schedule of RES hydrogen production system with downstream constraints. Int J Hydrogen Energy 2025;102:68–79. https://doi.org/10.1016/j.ijhydene.2024.12.518.

[10] Trapani D, Marocco P, Gandiglio M, Santarelli M. Decarbonizing semiconductor manufacturing: cost-competitiveness of PV-based green hydrogen production. Smart Energy 2025;19:100192. https://doi.org/10.1016/j.segy.2025.100192.

[11] Farah S, Bokde N, Andresen GB. Cost and CO 2 emissions co-optimisation of green hydrogen production in a grid-connected renewable energy system. Int J Hydrogen Energy 2024;84:164–76. https://doi.org/10.1016/j.ijhydene.2024.08.062.

[12] Silvente J, Kopanos GM, Pistikopoulos EN, Espuña A. A rolling horizon optimization framework for the simultaneous energy supply and demand planning in microgrids. Appl Energy 2015;155:485–501. https://doi.org/10.1016/j.apenergy.2015.05.090.

[13] Liao M, Liu C, Marocco P, Gandiglio M, Santarelli M. Optimal dispatch model for grid-connected wind-electrolysis plants. Int J Hydrogen Energy 2025;100:971–81. https://doi.org/10.1016/j.ijhydene.2024.12.200.

[14] Matute G, Yusta JM, Beyza J, Monteiro C. Optimal dispatch model for PV-electrolysis plants in self-consumption regime to produce green hydrogen: a Spanish case study. Int J Hydrogen Energy 2022;47:25202–13. https://doi.org/10.1016/j.ijhydene.2022.05.270.

[15] Zheng Y, You S, Bindner HW, Münster M. Optimal day-ahead dispatch of an alkaline electrolyser system concerning thermal–electric properties and state-transitional dynamics. Appl Energy 2022;307:118091. https://doi.org/10.1016/j.apenergy.2021.118091.

[16] Zheng Y, Huang C, Tan J, You S, Zong Y, Træholt C. Off-grid wind/hydrogen systems with multi-electrolyzers: optimized operational strategies. Energ Conver Manage 2023;295:117622. https://doi.org/10.1016/j.enconman.2023.117622.

[17] Ibáñez-Rioja A, Järvinen L, Puranen P, Kosonen A, Ruuskanen V, Hynynen K, et al. Off-grid solar PV–wind power–battery–water electrolyzer plant: simultaneous optimization of component capacities and system control. Appl Energy 2023;345:121277. https://doi.org/10.1016/j.apenergy.2023.121277.

[18] Bukar AL, Chaitusaney S, Kawabe K. Optimal energy management and techno-economic assessment of hydrogen energy production system incorporated with photovoltaic and battery storage. Int J Hydrogen Energy 2024;62:1139–53. https://doi.org/10.1016/j.ijhydene.2024.03.058.

[19] Mößle P, Herrmannsdörfer T, Welzl M, Brüggemann D, Danzer MA. Economic optimization for the dynamic operation of a grid connected and battery-supported electrolyzer. Int J Hydrogen Energy 2025;100:749–59. https://doi.org/10.1016/j.ijhydene.2024.12.216.

[20] Peng C, Wu Y, Zhang Y, Wang Z, Xue F, Xu H. Coordinated dispatch of alkaline and PEM electrolyzers: a stochastic optimization approach under renewable energy uncertainty. Int J Hydrogen Energy 2025;193:152237. https://doi.org/10.1016/j.ijhydene.2025.152237.

[21] Karthikeyan B, Praveen Kumar G, Basa S, Sinha S, Tyagi S, Kamat P, et al. Strategic optimization of large-scale solar PV parks with PEM Electrolyzer-based hydrogen production, storage, and transportation to minimize hydrogen delivery costs to cities. Appl Energy 2025;377:124758. https://doi.org/10.1016/j.apenergy.2024.124758.

[22] Wei M, Chen J, Zhang W, Chen Y, Zhang K, Lin D. Two-layer multi-timescale rolling optimization of electric-hydrogen hybrid energy storage systems considering renewable energy uncertainties. Int J Hydrogen Energy 2025;106:305–17. https://doi.org/10.1016/j.ijhydene.2025.01.435.

[23] Chen Z, Li Z, Lin D, Xie C, Wang Z. Multi-time-scale optimal scheduling of integrated energy system with electric-thermal-hydrogen hybrid energy storage under wind and solar uncertainties. Journal of Modern Power Systems and Clean Energy 2024;13:904–14. https://doi.org/10.35833/MPCE.2024.000606.

[24] Yang Z, Ren Z, Li H, Sun Z, Feng J, Xia W. A multi-stage stochastic dispatching method for electricity-hydrogen integrated energy systems driven by model and data. Appl Energy 2024;371:123668. https://doi.org/10.1016/j.apenergy.2024.123668.

[25] Wang J, Wen J, Wang J, Yang B, Jiang L. Water electrolyzer operation scheduling for green hydrogen production: a review. Renew Sustain Energy Rev 2024;203:114779. https://doi.org/10.1016/j.rser.2024.114779.

[26] Zier M, Stenzel P, Kotzur L, Stolten D. A review of decarbonization options for the glass industry. Energy Conversion and Management: X 2021;10:100083. https://doi.org/10.1016/j.ecmx.2021.100083.

[27] Thiry Z, Wan PK, Fragapane G. Lessons learned from hydrogen testing in glass production with hydrogen tube trailers as a supply method: a multiple case study. IFAC-PapersOnLine 2025;59:578–83. https://doi.org/10.1016/j.ifacol.2025.09.099.

[28] Diesing P, Lopez G, Blechinger P, Breyer C. From knowledge gaps to technological maturity: a comparative review of pathways to deep emission reduction for energy-intensive industries. Renew Sustain Energy Rev 2025;208:115023. https://doi.org/10.1016/j.rser.2024.115023.

[29] Solomon MD, Heineken W, Scheffler M, Birth-Reichert T. Cost optimization of compressed hydrogen gas transport via trucks and pipelines. Energy Tech 2024;12:2300785. https://doi.org/10.1002/ente.202300785.

[30] Marocco P, Gandiglio M, Cianella R, Capra M, Santarelli M. Design of hydrogen production systems powered by solar and wind energy: an insight into the optimal size ratios. Energ Conver Manage 2024;314:118646. https://doi.org/10.1016/j.enconman.2024.118646.

[31] Ember. European Wholesale Electricity Price Data. 2026.

[32] IRENA. Renewable power generation costs in 2024. 2025.

[33] Economics Trading. EU carbon permits. https://tradingeconomics.com/commodity/carbon; 2025.

[34] Electricity maps portal. Interactive map 2025. https://app.electricitymaps.com/map/live/fifteen_minutes.

[35] Clean air task force. Hydrogen production calculator 2023. https://www.catf.us/hydrogen-converter/#units [accessed October 20, 2025].

[36] Hasturk U, Schrotenboer AH, Ursavas E, Roodbergen KJ. Stochastic cyclic inventory routing with supply uncertainty: a case in green-hydrogen logistics. Transportation Science 2024;58:315–39. https://doi.org/10.1287/trsc.2022.0435.

[37] Reksten AH, Thomassen MS, Møller-Holst S, Sundseth K. Projecting the future cost of PEM and alkaline water electrolysers; a CAPEX model including electrolyser plant size and technology development. Int J Hydrogen Energy 2022;47:38106–13. https://doi.org/10.1016/j.ijhydene.2022.08.306.

[38] European Hydrogen Observatory. Cost of hydrogen production. https://observatory.clean-hydrogen.europa.eu/hydrogen-landscape/production-trade-and-cost/cost-hydrogen-production#:~:text=Hydrogen%20production%20costs%20via%20electrolysis; 2024. median%20of%206.20%20EUR%2Fkg (accessed October 20, 2025).

[39] Eurostat. Wages and labour costs. 2023. https://ec.europa.eu/eurostat/statistics-explained/index.php?title=Wages_and_labour_costs#Labour_costs (accessed February 11, 2025).

[40] Zhang Y, Sahinidis NV. Solving continuous and discrete nonlinear programs with BARON. Comput Optim Appl 2025;92:1123–61. https://doi.org/10.1007/s10589-024-00633-0.